Pion double charge exchange in the Δ_{33} resonance region

A. Wirzba
Nordisk Institut for Teoretisk Atomfysik, Blegdamsvej 17, DK-2100 Copenhagen, Denmark

H. Toki
Tokyo Metropolitan University, Tokyo 158, Japan

E. R. Siciliano and Mikkel B. Johnson
Los Alamos National Laboratory, Los Alamos, New Mexico 87545

R. Gilman*
University of Pennsylvania, Philadelphia, Pennsylvania 19104
(Received 16 June 1989)

We examine the model dependence and nuclear-structure sensitivity of several Δ_{33}-dominated processes contributing to pion double charge exchange on nuclei in the region of the Δ_{33} resonance. These processes include the Δ_{33}-nucleon interaction $V_{N\Delta}$ and sequential scattering, in which the pion undergoes single charge exchange on two different nucleons. In all cases, the scattering takes place through the exchange of an intermediate π and ρ meson. Sequential-mediated double charge exchange is found to be only moderately sensitive to short-range correlations, meson-nucleon form factors, and the rho meson, whereas $V_{N\Delta}$-mediated double charge exchange is very sensitive to all these effects. Results are given for double charge exchange on ^{18}O (double isobaric analog transitions) and ^{16}O (nonanalog transitions). Sequential double charge exchange is shown to favor non-spin-flip matrix elements of the transition operator whereas $V_{N\Delta}$-mediated double charge exchange favors spin-flip matrix elements. The energy dependence of the zero-degree cross sections for $V_{N\Delta}$ and sequential scattering are also different: Sequential tends to increase monotonically from 100 to 300 MeV, whereas $V_{N\Delta}$ peaks at about 150 MeV. The delta-nucleon interaction is found likely to dominate over sequential scattering in nonanalog double charge exchange. The $V_{N\Delta}$ is also large in analog double charge exchange, but it does not enable us to explain the anomalous behavior of the ^{18}O differential cross sections.

I. INTRODUCTION

The first excited state of the nucleon, the Δ_{33}, plays an essential role in the dynamics of nuclear many-body systems. Once the Δ_{33} is excited as a real or virtual particle in the nucleus it may interact with nucleons through the Δ_{33}-nucleon interaction $V_{N\Delta}$. Phenomenological studies have shown that this interaction can be important both in pion elastic scattering[1,2] and in nuclear structure.[3] However, it has been difficult to make reliable calculations because the details of the interaction are rather uncertain. Consequently, theoretical and experimental studies capable of a more direct determination of $V_{N\Delta}$ are quite important. The pion double-charge-exchange (DCX) reaction appears to be one place where such an opportunity exists.[4–8] In previous work we have presented results of coupled-channel[4] and distorted-wave impulse-approximation (DWIA) calculations[5,6] supporting this observation, and in this paper we want to provide a more thorough study of the contribution of $V_{N\Delta}$ to pion DCX in the DWIA framework.

There are two classes of DCX reactions that have been measured. One of these is the excitation of the double isobaric analog state, in which two excess neutrons in a nucleus of total isospin $T \geq 1$ are converted into two protons in the same space-spin orbitals.[9] The second is the nonanalog transition, for which the space-spin orbitals of the neutrons change, leaving the final nucleus in its ground state.[10] Experimental results for these two classes of reactions exist for many nuclei over a wide range of energies,[9–11] and we will study both classes in this paper. Because we are interested in the Δ_{33}-dominated processes, our work focuses on the energies for which the Δ_{33} is strongly excited, i.e., pion kinetic energies of 100 MeV $\lesssim T_\pi \lesssim$ 300 MeV.

Figure 1(a) depicts DCX occurring through a successive interaction of the Δ_{33} on the same nucleon. This may be viewed as double charge exchange through the isovector, π-plus ρ-meson-exchange part of the Δ_{33}-nucleon interaction (DINT). This process is the main focus of our paper. Two closely related processes are shown in Figs. 1(b)–(c). These Δ_{33} wave-function processes (DWF) allow a Δ_{33} to exist in the nucleus after (before) the pion scatters, and they may be evaluated quantitatively using the same methods developed for Fig. 1(a). Figure 1(d) is the sequential process (SEQ) in which double charge exchange occurs as a result of single-charge-exchange processes on two different nucleons. Although

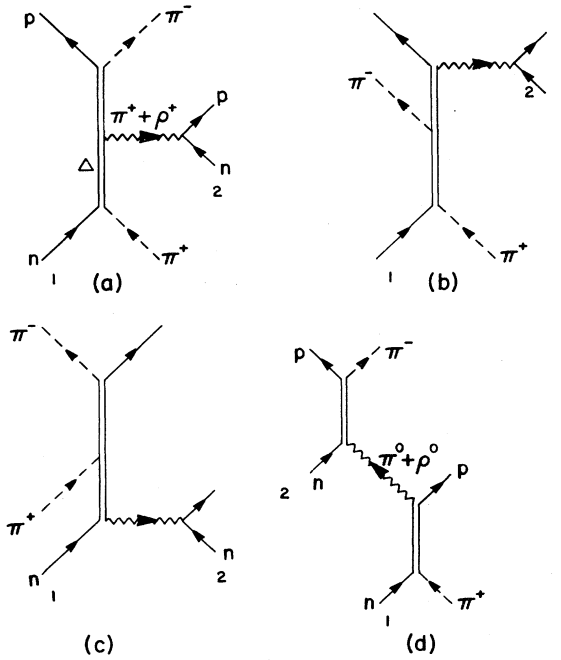

FIG. 1. Feynman diagrams for the DCX reactions involving Δ isobar dynamics. (a) The pion scatters from one nucleon while its charge is transferred to the second nucleon by the Δ_{33}-nucleon interaction (DINT); (b) and (c). The pion excites a Δ_{33}, which is in the nuclear wave function after (before) the scattering has occurred (DWF); (d) The pion undergoes sequential single-charge-exchange scatterings on two different nucleons (SEQ).

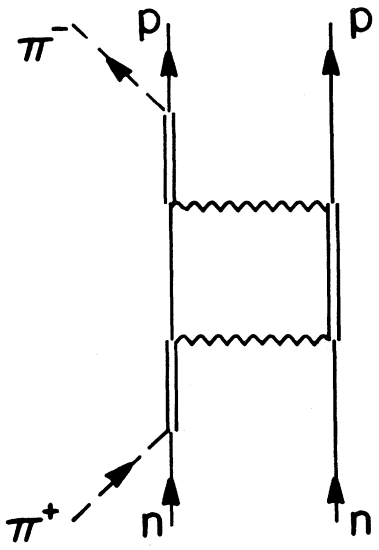

FIG. 2. A Feynman diagram for the DCX reaction, in which two mesons are exchanged between the intermediate Δ isobar and nucleon. This and other closely related two-meson-exchange pieces of the Δ_{33}-nucleon interaction are not taken into account in this paper, but might be important.

the DWIA methods used for Figs. 1(a)–(c) are not as well suited to evaluate the absolute magnitude of the SEQ process in the regime of strong absorption, discussing it in the same framework will provide insight into the physics of all Δ_{33}-dominated processes and will enable us to make some estimates that qualitatively reflect the physics of SEQ process.

The terms in Fig. 1(a) and (d) represent two important pieces of the Δ_{33}-nucleon interaction. In addition to these there are two-meson-exchange pieces (e.g., Fig. 2) that may be large.[12] At smaller separations of the two nucleons, the Δ_{33}-N interaction may require explicit introduction of quarks and gluons[13,14] (see Fig. 3). The more complicated pieces need to be considered in order to completely understand $V_{N\Delta}$, but they will not be considered further in this paper.

The paper is organized as follows. In Sec. II we state our underlying model of the meson-baryon couplings and make a decomposition of the terms in Fig. 1 into seven tensors which contribute to ground-state transitions (with total angular momentum I equal to zero). In Sec. III we show how this is embedded into a distorted-wave impulse-approximation calculation to obtain DCX cross sections. Section IV presents some of the details of the evaluation of transition densities and shows the sensitivity of the cross sections to various quantities that characterize our model. In Sec. V we combine the results studied separately in Sec. IV and show numerical results using shell-model wave functions. Finally, in Sec. VI we summarize our findings and discuss future possibilities.

II. MODEL AND TENSORAL DECOMPOSITION

We assume that the nucleons are fixed sources and that the π- and ρ-meson fields couple to the nucleon and Δ_{33} as shown in Fig. 4 by the following matrix elements

$$\pi\text{:}\quad \frac{f_\pi}{m_\pi}\mathcal{S}\cdot\mathbf{k}\mathcal{T}\cdot\boldsymbol{\alpha}v_\pi(k) \tag{2.1}$$

$$\rho\text{:}\quad \frac{f_\rho}{m_\rho}\boldsymbol{\epsilon}\cdot\mathcal{S}\times\mathbf{k}\mathcal{T}\cdot\boldsymbol{\alpha}v_\rho(k)\ , \tag{2.2}$$

where $\mathbf{k}$ is the meson momentum, $\boldsymbol{\epsilon}$ is the ρ-meson polarization, $\boldsymbol{\alpha}$ is the meson isospin wave function, and $v(k)$ is a form factor taken to be a function of ω and $\mathbf{k}$,

$$v(k)=(\Lambda^2-m^2)/(\Lambda^2-\omega^2+\mathbf{k}^2)\ , \tag{2.3}$$

where ω is the total energy of the meson. These couplings are depicted diagrammatically in Fig. 4. We choose one cutoff Λ_π for all processes involving the π and one, Λ_ρ, for the ρ meson. The operator $\mathcal{S}$ is the Pauli spin matrix $\boldsymbol{\sigma}$ for Fig. 4(a), the transition operator $\mathbf{S}$, for Fig. 4(b), and the spin $\frac{3}{2}$ operator $\boldsymbol{\Sigma}$ for Fig. 4(c) using the conventions of Ref. 4. The operators $\mathcal{T}$ are the corresponding isospin operators (i.e., $\boldsymbol{\tau}$, $\mathbf{T}$, and $\boldsymbol{\Theta}$ respectively). The coupling strengths are related by the SU(2)×SU(2) quark model and are[15]

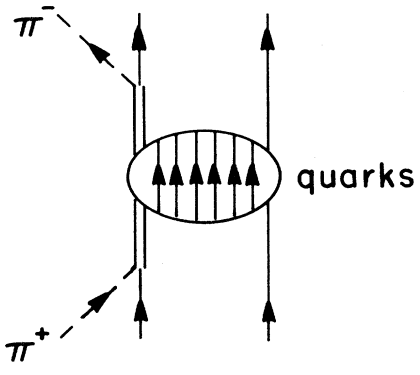

FIG. 3. The short-range part of the Δ-nucleon interaction, involving direct participation of the quark-gluon degrees of freedom.

$$f_{\pi N\Delta}/f_{\rho N\Delta}=f_{\pi\Delta\Delta}/f_{\rho\Delta\Delta}=f_{\pi NN}/f_{\rho NN}\ , \tag{2.4}$$

$$f_{\pi\Delta\Delta}/f_{\pi NN}=\tfrac{4}{5}\ . \tag{2.5}$$

The couplings $f_{\pi NN}$ and $f_{\pi N\Delta}$ are taken from experiment to be

$$f^2_{\pi NN}/4\pi=0.079 \tag{2.6}$$

and

$$f^2_{\pi N\Delta}/4\pi=0.37\ . \tag{2.7}$$

The ratio f_ρ/f_π that we use has been taken to be large in accord with modern one-boson-exchange models,

$$\left[\frac{f_\rho m_\pi}{f_\pi m_\rho}\right]^2=2.6\ , \tag{2.8}$$

but the precise value of this quantity depends in detail on the model as discussed further in Ref. 16.

The rules for evaluating diagrams may be found in Ref. 4. As an example, consider the DINT process of Fig. 1(a). Using the couplings in Eqs. (2.1)–(2.7), and denoting the diagrams by $\theta^{(i)}_{12}$ (i labels the different terms in Fig. 1 and the subscript 12 denotes the order in which the mesons interact with the nucleons) we find for the π-exchange piece

$$\begin{aligned}\theta^{1a}_{12}(\mathbf{k}',\mathbf{k};\mathbf{r}_1,\mathbf{r}_2)=\int\frac{d^3k''}{(2\pi)^3}\sum_{\alpha''}&\left[\frac{f_{\pi NN}}{m_\pi}\right]v_\pi(k'')\boldsymbol{\sigma}_2\cdot\mathbf{k}''\boldsymbol{\tau}_2\cdot\boldsymbol{\alpha}''\left[\frac{f_{\pi\Delta\Delta}}{m_\pi}\right]v_\pi(k'')\\&\times\frac{e^{i\mathbf{k}''\cdot(\mathbf{r}_2-\mathbf{r}_1)}}{-k''^2-m_\pi^2}\left[\frac{f_{\pi N\Delta}}{m_\pi}\right]^2 v_\pi(k')\mathbf{S}_1^+\cdot\mathbf{k}'\mathbf{T}_1^+\cdot\boldsymbol{\alpha}'\\&\times G^2_\Delta(\omega)\boldsymbol{\Sigma}_1\cdot\mathbf{k}''\boldsymbol{\Theta}\cdot\boldsymbol{\alpha}''\mathbf{T}_1\cdot\boldsymbol{\alpha}\mathbf{S}_1\cdot\mathbf{k}v_\pi(k)e^{-i\mathbf{r}_1\cdot(\mathbf{k}'-\mathbf{k})}\ .\end{aligned} \tag{2.9}$$

The propagator G_Δ is taken to be

$$G_\Delta(\omega)=\left[\sqrt{s}-M_\Delta+i\frac{W}{2}\right]^{-1} \tag{2.10}$$

with

$$M_\Delta=1232\ \text{MeV} \tag{2.11}$$

and

$$\frac{W(\omega)}{2}=\frac{M_n}{m_\pi^2}\frac{1}{3}\frac{f^2_{\pi N\Delta}}{4\pi}\frac{k^2}{\sqrt{s}}\ ,$$

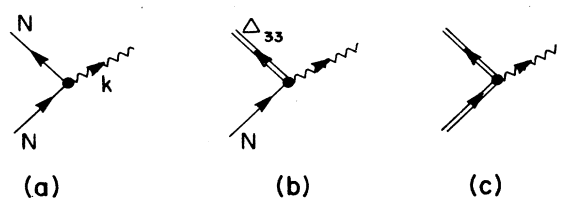

FIG. 4. NN-, $N\Delta$-, and $\Delta\Delta$-meson vertices. The wavy line denotes pions and ρ mesons.

where s is the total center-of-mass energy of the pion and nucleon and k is their center-of-mass momentum. Sometimes one uses a different expression for W; Eq. (2.11) is the one used in the comparisons of Ref. 8. The quantities $\boldsymbol{\alpha}'$, $\boldsymbol{\alpha}''$, and $\boldsymbol{\alpha}$ are the isospin wave functions for the final, intermediate, and initial pion. When applying the same set of rules to SEQ, Fig. 1(d), we automatically sum over all intermediate nuclear states by closure.

In order to use the processes of Fig. 1 for nuclear-physics calculations it is helpful to express them as tensors in the spin and isospin variables of the nucleons and the momentum and isospin variable of the mesons. In the sequential process of Fig. 1(d) we accomplish this by the identities

$$\mathbf{S}^+\cdot\mathbf{k}'\mathbf{S}\cdot\mathbf{k}''=\tfrac{2}{3}\mathbf{k}'\cdot\mathbf{k}''-(i/3)\boldsymbol{\sigma}\cdot\mathbf{k}'\times\mathbf{k}''\ , \tag{2.12}$$

$$\mathbf{T}^+\cdot\boldsymbol{\alpha}'\mathbf{T}\cdot\boldsymbol{\alpha}''=\tfrac{2}{3}\boldsymbol{\alpha}'\cdot\boldsymbol{\alpha}''-(i/3)\boldsymbol{\tau}\cdot\boldsymbol{\alpha}'\times\boldsymbol{\alpha}''\ . \tag{2.13}$$

The isospin matrix elements may be written in terms of the operator $\boldsymbol{\phi}$ of the pion by using the relationships

$$\boldsymbol{\alpha}'\cdot\boldsymbol{\alpha}=\langle\alpha'|\alpha\rangle \tag{2.14}$$

$$\boldsymbol{\tau}\cdot\boldsymbol{\alpha}'\times\boldsymbol{\alpha}=i\langle\alpha'|\boldsymbol{\phi}|\alpha\rangle\cdot\boldsymbol{\tau}\ . \tag{2.15}$$

The identities corresponding to Eqs. (2.12) and (2.13) that are needed for DINT and DWF are given in Ref. 4.

Next, we collect the spin and isospin operators into the isotensor τ_{12}

$$\tau_{12}=\tfrac{1}{2}(\tau_1\cdot\boldsymbol{\phi}\tau_2\cdot\boldsymbol{\phi}+\tau_2\cdot\boldsymbol{\phi}\tau_1\cdot\boldsymbol{\phi}) \tag{2.16}$$

and $M(\lambda\alpha\lambda'\beta)$

$$M(\lambda\alpha\lambda'\beta)=[[\mathbf{k}'\otimes\mathbf{k}]^{\lambda}\otimes[Y_{\alpha}(\hat{\mathbf{k}}'')\otimes S_{\beta}^{\lambda'}(\boldsymbol{\sigma}_1,\boldsymbol{\sigma}_2)]^{\lambda}]^{0}(-)^{\lambda} \tag{2.17}$$

with

$$S_{\beta}^{\lambda'}=\delta(\lambda',0)\quad\beta=0\ , \tag{2.18}$$

$$S_{\beta}^{\lambda'}=[\boldsymbol{\sigma}_1\otimes\boldsymbol{\sigma}_2]^{\lambda'}\quad\beta=1\ . \tag{2.19}$$

The index α in Eq. (2.17) is restricted to the values 0 and 2 because we have considered only p-wave couplings in Eqs. (2.1) and (2.2). The bracket $[\ ]^{\lambda}$ indicates an irreducible spherical tensor[17] of rank λ. The manipulations involved in this process are quite tedious, but in the end the result has a simple form. We define

$$e^{-i\mathbf{q}\cdot\mathbf{R}}D_i(\mathbf{k}',\mathbf{k};\mathbf{r})\equiv\theta_{12}^{(i)}+\theta_{21}^{(i)} \tag{2.20}$$

retaining the 2 orders of interaction of the pion with the nucleons. In Figs. 5 and 6 and Appendix A we verify that the counting works out properly in the end. [The quantity $e^{-i\mathbf{q}\cdot\mathbf{R}}D_i$ in Eq. (2.20) is called $\hat{D}_i$ in Ref. 18. For the purpose of treating distortions in Sec. III, it is convenient to pull out the phase as we do here.] We then write

$$D_i(\mathbf{k}',\mathbf{k};r)=\tfrac{2}{3}\sqrt{4\pi}v(k')v(k)e^{i\mathbf{Q}\cdot\mathbf{r}}\tau_{12}\sum_{\substack{\lambda\alpha\lambda'\\ \beta}}i^{-\alpha}a_i(\lambda\alpha\lambda'\beta)\int\frac{d^3k''}{(2\pi)^3}\frac{k''^2v^2(k'')e^{i\mathbf{k}''\cdot\mathbf{r}}}{\bar{k}_{\pi}^{\,2}-k''^2+i\eta}M(\lambda\alpha\lambda'\beta)\ , \tag{2.21}$$

where $\mathbf{q}=\mathbf{k}'-\mathbf{k}$, $\mathbf{r}=\mathbf{r}_2-\mathbf{r}_1$, and $\mathbf{R}=(\mathbf{r}_1+\mathbf{r}_2)/2$. The coefficients $a_i(\lambda\alpha\lambda'\beta)$ are given in Table I, and $\mathbf{Q}$ and $\bar{k}_{\pi}^{\,2}$ are defined in Table II. The results given here for DINT and DWF are also found in Ref. 4, but one should note that a different normalization of the tensors was used in the earlier paper. (This accounts for the differences between the coefficients in our Table I and those in Table II of Ref. 4.) The factor of $\frac{2}{3}$ in Eq. (2.21) has been pulled out of a_i for historical reasons and has no special significance. In deriving these results it is useful to note that for pion double charge exchange, the tensors odd in τ_1 and τ_2 (e.g., $\tau_1-\tau_2$) may be omitted because the pair on which DCX occurs (neutron-neutron or proton-proton) is symmetric in these variables. The tensors having $\lambda=1$, for example $\boldsymbol{\sigma}_1\times\boldsymbol{\sigma}_2$, $\boldsymbol{\sigma}_1+\boldsymbol{\sigma}_2$, and $\boldsymbol{\sigma}_1-\boldsymbol{\sigma}_2$ have been omitted from consideration because they do not contribute to the analog and nonanalog transitions for the cases considered here. In this case θ_{12} and θ_{21} each give the same contribution to D_i in Eq. (2.21). A more complete treatment of the spin, which is needed when the initial or final nucleus has spin, will be considered in Ref. 18.

One of the main differences between DINT and DWF on the one hand and SEQ on the other is the dynamics of the intermediate pion propagation. In the former processes, the pion can be treated as a potential-like exchange because it is virtual. However, in the latter case, the intermediate pion is on-shell and can propagate over large distances unless it is damped by absorption. The sequential mechanism is therefore subject to the medium modifications of a real pion. We are able to include these intermediate distortions in an average sense through the pion self-energy Σ in the nuclear medium of density $\rho(R)$,

$$\Sigma=-4\pi\rho(\bar{R})f(0)\ , \tag{2.22}$$

where $f(0)$ is the pion-nucleon scattering amplitude, and where $\bar{R}$ is the average center-of-mass radius at which the (τ^+,π^-) transitions takes place. For analog transitions we have chosen $\bar{R}$ in Eq. (2.22) to normalize the cross section in a manner discussed in Sec. IV.

The integral over $\mathbf{k}''$ in Eq. (2.21) may now be expressed in terms of the function $H_L(\bar{k},r)$ defined as

$$H_L(\bar{k},r)=-\frac{2}{\pi i\bar{k}^{\,3}}\int\frac{t^4dt\,j_L(tr)}{\bar{k}^{\,2}-t^2+i\eta}\frac{v^2(t)}{v^2(\bar{k})}\ . \tag{2.23}$$

These functions are tabulated analytically in Ref. 19.

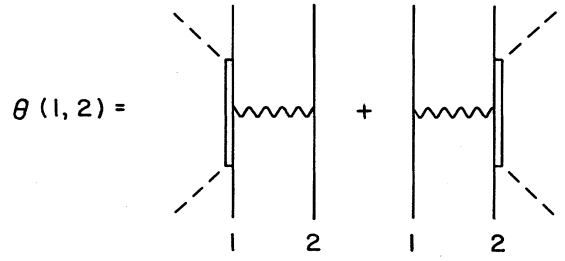

FIG. 5. Two-body operator acting on particles 1 and 2.

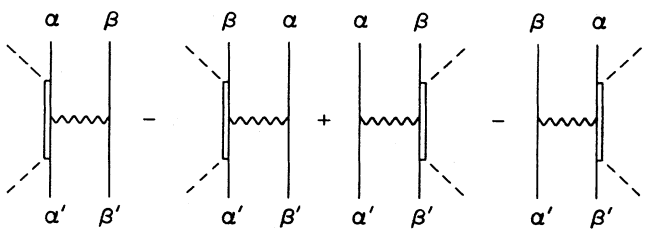

FIG. 6. Four distinct amplitudes corresponding to the expectation value in Eq. (A2).

TABLE I. Coefficients of tensors in Eq. (2.21). The four coefficients a_1, a_2, a_3, and a_4 correspond to diagrams in Fig. 1(a), (b), (c), and (d), respectively. The constants c_1, c_2, c_3, and c_4 are defined in Table II.

j	λ	α	λ'	β	a_1/c_1	a_2/c_2	a_3/c_3	a_4/c_4
1	0	0	0	0				$-4\sqrt{3}/81$
2	0	0	0	1	5/9			$\frac{2}{81}$
3	2	2	0	0				$-4\sqrt{6}/81$
4	2	2	0	1	$-\sqrt{2}/9$	$-\sqrt{2}/4$	$-\sqrt{2}/4$	$-\sqrt{2}/81$
5	2	0	2	1	$-\sqrt{5}/9$	$-\sqrt{5}/4$	$-\sqrt{5}/4$	$-\sqrt{5}/81$
6	0	2	2	1	$+5\sqrt{2}/9$			$-\sqrt{2}/81$
7	2	2	2	1	$-\sqrt{14}/18$	$-\sqrt{14}/8$	$-\sqrt{14}/8$	$\sqrt{14}/81$

$D_i(\mathbf{k}',\mathbf{k};\mathbf{r})$ becomes

$$D_i(\mathbf{k}',\mathbf{k};\mathbf{r})=\sum_{\substack{\lambda\alpha\lambda'\\ \beta}}(-)^{\lambda}d_i(\alpha,\mathbf{r})A_i(\lambda\alpha\lambda'\beta)\times[[\mathbf{k}'\otimes\mathbf{k}]^{\lambda}\otimes[Y_{\alpha}(\hat{\mathbf{r}})\otimes S_{\beta}^{\lambda'}]^{\lambda}]^{0}\ , \tag{2.24}$$

where

$$d_i(\alpha,\mathbf{r})=i\frac{\bar{k}_{\pi}^{3}v_{\pi}^{2}(\bar{k}_{\pi})}{m_{\pi}^{3}}e^{i\mathbf{Q}\cdot\mathbf{r}}H_{\alpha}(\bar{k}_{\pi},r)\Gamma(r)\ , \tag{2.25}$$

$$A_i=-\frac{2}{3}\frac{m_{\pi}^{3}}{\sqrt{4\pi}}\tau_{12}a_i(\lambda\alpha\lambda'\beta)v(k')v(k)\ . \tag{2.26}$$

Here, we have added the short-range correlation function $\Gamma(r)$. For calculations in this paper we choose the correlation function to be the same as that for two nucleons,

$$\Gamma(r)=1-j_0(m_0r) \tag{2.27}$$

with $m_0=780$ MeV in accordance with NN G-matrix calculations.[20] Because our results are quite sensitive to $\Gamma(r)$ (Sec. V), it would be desirable to take $\Gamma(r)$ from a $N\Delta$ G-matrix calculation. To our knowledge, such a calculation does not exist at this time.

The ρ meson may be evaluated easily by recognizing that the ρ meson in Fig. 1 contributes to the spin-spin force (which is proportional to H_0) and to the tensor force (which is proportional to H_2). These are simple contractions of k'' with the operator $\mathcal{S}$ [see Eqs. (2.1) and (2.2)]. The relationship between the pion and ρ-meson spin-spin and tensor force is the same as for the NN force so we make the replacement

$$H_{\alpha}(\bar{k}_{\pi},r)\rightarrow H_{\alpha}(\bar{k}_{\pi},r)+2.6\left[\frac{\bar{k}_{\rho}}{\bar{k}_{\pi}}\right]^{3}\frac{v_{\rho}^{2}(\bar{k}_{\rho})}{v_{\pi}^{2}(\bar{k}_{\pi})}\begin{Bmatrix}2 & \alpha=0\\ -1 & \alpha=2\end{Bmatrix}H_{\alpha}(\bar{k}_{\rho},r)\ , \tag{2.28}$$

where $\bar{k}_{\rho}$ is given in Table II. The factor of 2.6 in Eq. (2.28) arises from the ratio of π- to ρ-meson coupling constants given in Eq. (2.8), and the factors 2 and -1 correspond to the well-known fact that the ρ-meson enhances the spin-spin force but weakens the tensor force. The value $m_{\rho}=644$ MeV is used in evaluating $\bar{k}_{\rho}$ and $v_0(k)$ in Eq. (2.28). The mass is reduced to approximately account for the uncorrelated 2π exchange.[16]

III. DWIA MATRIX ELEMENTS

The amplitude $\tilde{\mathcal{F}}^{i}$ corresponding to a diagram D_i in Fig. 1 is

$$\tilde{\mathcal{F}}^{i}(\mathbf{k}_0',\mathbf{k}_0)=\int\chi^{*(-)}(\mathbf{k}_0',\mathbf{R})\langle\psi_{Nf}|D_i(\mathbf{k}',\mathbf{k};\mathbf{r}')\delta(\mathbf{R}'-\mathbf{R})|\psi_{Ni}\rangle\chi^{(+)}(\mathbf{k}_0,\mathbf{R})d^{3}\mathbf{R}\ , \tag{3.1}$$

TABLE II. Values for c_i appearing in Table I and values of $\mathbf{Q}$ and $\bar{k}_{\pi}^{2}$ appearing in Eq. (2.21). Also given are the values of $\bar{k}_{\rho}^{2}$ in Eq. (2.28). The value of Σ is the pion self-energy and is discussed in the text. Here $k_0^2=\omega^2-m_{\pi}^2$.

Diagram	$c_i/(f_{\pi NN}^2/m_{\pi}^2)^2$	$\mathbf{Q}$	$\bar{k}_{\pi}$	$\bar{k}_{\rho}$
1	$\left[\frac{f_{\pi N\Delta}}{f_{\pi NN}}\right]^2\left[\frac{f_{\pi\Delta\Delta}}{f_{\pi NN}}\right]G_{\Delta}^{2}(\omega)$	$\mathbf{q}/2$	im_{π}	im_{ρ}
2	$\left[\frac{f_{\pi N\Delta}}{f_{\pi NN}}\right]^2\left[\frac{f_{\pi\Delta\Delta}}{f_{\pi NN}}\right]G_{\Delta}(\omega)G_{\Delta}(0)$	$\mathbf{q}/2$	im_{π}	im_{ρ}
3	$\left[\frac{f_{\pi N\Delta}}{f_{\pi NN}}\right]^2\left[\frac{f_{\pi\Delta\Delta}}{f_{\pi NN}}\right]G_{\Delta}(\omega)G_{\Delta}(0)$	$\mathbf{q}/2$	im_{π}	im_{ρ}
4	$\left[\frac{f_{\pi N\Delta}}{f_{\pi NN}}\right]^4G_{\Delta}^{2}(\omega)$	$(\mathbf{k}+\mathbf{k}')/2$	$(k_0^2-\Sigma)^{1/2}$	$i(m_{\rho}^2-m_{\pi}^2-k_0^2)^{1/2}$

where $\chi^{(-)}(\mathbf{k}_0',\mathbf{R})$ and $\chi^{(+)}(\mathbf{k}_0,\mathbf{R})$ are, respectively, the outgoing and incoming distorted waves corresponding to pions of asymptotic momenta $\mathbf{k}_0'$ and $\mathbf{k}_0$. In this expression $\mathbf{r}'$ and $\mathbf{R}'$ are the relative and center-of-mass coordinates of the two nucleons on which double charge exchange takes place and are integration variables in the nuclear matrix element. The delta function expresses the requirement that $\mathbf{r}'$ in this matrix element function is integrated holding the center-of-mass coordinate in the wave function fixed at R. The cross section is given by

$$d\sigma/d\Omega=|\sum_i \tilde{\mathcal{F}}^i/4\pi|^2 .$$

To obtain Eq. (3.1) we have replaced the initial and final plane waves $e^{-i\mathbf{q}\cdot\mathbf{R}}$ in Eq. (2.20) by distorted waves. This replacement is motivated by the short-range character of DINT and DWF. It is justified for SEQ only in a qualified sense. Whereas this approximation confines the reaction to the surface as required when pion attenuation is included, it does not pay sufficient attention to the geometry of the surface. As a result, the important characteristics of diffraction, namely straight-line trajectories and the consequential suppression of transitions for which $l\neq l'$, are not expected to be realized at the two single-charge-exchange scatterings in Fig. 1(d). Transitions for which $l\neq l'$ play a prominent role in nonanalog transitions, and for this reason we do not believe that our SEQ can be applied without modification to study ^{16}O. However, they play a relatively minor role in analog transitions, so we believe that our results for SEQ will not be misleading in our study of ^{18}O. As written in Eq. (2.21), D_i is a highly nonlocal operator in $\mathbf{k}$ and $\mathbf{k}'$. How we handle the nonlocalities is indicated at the end of this section. The states $|\psi_N\rangle$ are the nuclear wave functions, for which we choose shell-model states in our comparisons to the data.

Our calculations are performed in coordinate space. To evaluate $\tilde{\mathcal{F}}_i$, we use a modified version of the computer program DWPI.[21] For the distortions in the DWIA calculations, we have used the optical-model program PIESDEX, described elsewhere.[22] We have made comparisons of DINT to the results of an independent momentum-space calculation[8] in which distortions were evaluated using semi-classical Glauber-model pion wave functions. We found amplitudes for DINT that were nearly the same in the two approaches in the plane-wave limit. This serves as an important check on the derivation of our DINT results. The plane-wave results for SEQ did not agree, but this was expected due to the elimination of spin flip in the SEQ calculation of Ref. 8. However, as described in Sec. IV of this paper, we have achieved agreement between our SEQ calculations and coupled-channel results, and this serves as an independent check on our SEQ.

In our studies in Ref. 8 we could not obtain agreement with DINT when the pion distorted waves were used. However, similar difficulties in obtaining agreement between optical-model and semi-classical calculations were found in previous work.[22] It was shown there that corrections to the semi-classical approximation for energies less than about 300 MeV are substantial due to the fact that the pion wave number is still quite large, and it can easily be seen from the results given there that the semi-classical approximation tends to underestimate the pion distortions below resonance and overestimate them above resonance.

The numerical results that we show in this paper use a particularly simple prescription for the optical potential, namely an average of the free pion-nucleon amplitude over the ground-state density inferred from electron scattering and corrected for the finite size of the proton. Typical reproductions of elastic scattering corresponding to the distortions $\chi^{\pm}$ are shown in Fig. 7. The quality of the fit can be improved by using an energy shift,[23] but this does not change the conclusions reached in this paper.

Consider first the effective transition density $\mathcal{F}_{12}^i$ for a pair of nucleons evaluated in a single-particle basis,

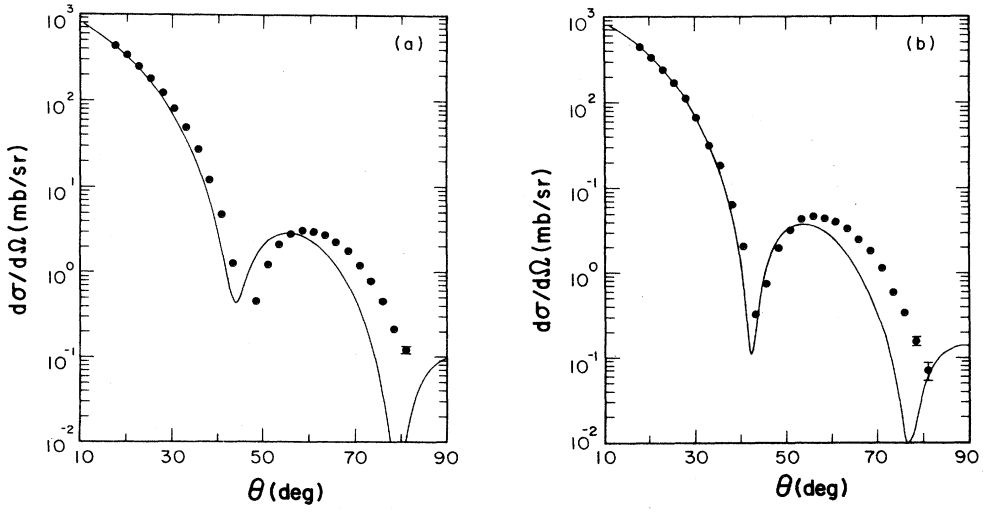

FIG. 7. Elastic-scattering angular distributions of π^+ (a) and π^- (b) on ^{18}O at $T_\pi=164$ Mev.

$$\mathcal{F}^i_{12}=\langle j'_1 m'_1 j'_2 m'_2|D_i(\mathbf{k}',\mathbf{k};\mathbf{r}')\delta(\mathbf{R}'-\mathbf{R})|j_1 m_1 j_2 m_2\rangle \quad (3.2)$$

with D_i given in Eq. (2.24). It is, of course, understood that the initial (final) state in Eq. (3.2) consists of two neutrons (protons) for incident π^+ (π^-). The corresponding many-body operator that results from expanding in terms of states coupled to a total angular momentum may be written in second-quantized notation

$$\hat{\mathcal{F}}^i=\frac{1}{2}\sum_{J'M'}\sum_{JM}(a^+_{j'_1}a^+_{j'_2})^{J'M'}\langle(j'_1j'_2)J'M'|D_i(\mathbf{k}',\mathbf{k};\mathbf{r}')\delta(\mathbf{R}'-\mathbf{R})|(j_1j_2)JM\rangle(\tilde{a}_{j_2}\tilde{a}_{j_1})^{J-M}(-)^{-J+M}, \quad (3.3)$$

where $\tilde{a}_{j,m}\equiv(-)^{j+m}a_{j,-m}$ and $(a^+_{j_2}a^+_{j_1})^{J,M}$ means that a pair of protons is created with angular momentum J,M. (We suppress the sum over single-particle labels and isospin quantum numbers for simplicity.)

Expanding the delta function in Eq. (3.2) and recoupling, we may write $\mathcal{F}^i$ in the alternative convenient form

$$\mathcal{F}^i=\sum_{\lambda\alpha\lambda'\beta}A_i(\lambda\alpha\lambda'\beta)\sum_{K\Lambda M_K}\frac{(-)^{\Lambda+K+M_K+\lambda}}{\sqrt{2\lambda+1}}\{Y_\Lambda(\hat{\mathbf{R}})\otimes[\mathbf{k}'\otimes\mathbf{k}]^\lambda\}^K_{-M_K}f_{KM_K}(\lambda\alpha\lambda'\beta;\Lambda,R), \quad (3.4)$$

where

$$f_{KM_K}(\lambda\alpha\lambda'\beta;\Lambda,R)\equiv\langle(j'_1j'_2)J'M'|d_i(\alpha,\mathbf{r}')\frac{\delta(R'-R)}{R^2}[Y_\Lambda(\hat{\mathbf{R}}')\otimes[Y_\alpha(\hat{\mathbf{r}}')\otimes S^{\lambda'}_\beta(\boldsymbol{\sigma}_1,\boldsymbol{\sigma}_2)]^\lambda]^K_{M_K}|(j_1j_2)JM\rangle . \quad (3.5)$$

In deriving Eq. (3.5), we have used a zero-range approximation, i.e., replaced $e^{i\mathbf{Q}\cdot\mathbf{r}}$ in Eq. (2.25) by $j_0(Qr)$. We may then define a reduced matrix element $f_K(\lambda\alpha\lambda'\beta;\Lambda,R)$ as

$$f_{KM_K}(\lambda\alpha\lambda'\beta;\Lambda,R)\equiv(-)^{2K}\langle J'M'|JKMM_K\rangle f_K(\lambda\alpha\lambda'\beta;\Lambda,R) . \quad (3.6)$$

The corrections to the zero-range approximation used in deriving Eq. (3.5) are obtained in Appendix B, and the importance of these corrections is examined in Appendix C. One expects corrections to become necessary when $Q\langle r\rangle\gtrsim 1$, where $\langle r\rangle$ is the range of the exchanged meson. For DINT and DWF in the plane-wave impulse approximation, this occurs only at large angles because $\mathbf{Q}=\mathbf{q}/2$ where $\mathbf{q}$ is the momentum transfer (Table II) and r is bounded because of the finite range of the π- and ρ-meson-exchange interaction. When distorted waves are used, we find in Appendix C that the corrections remain small for DINT. For SEQ, neither $|\mathbf{Q}|$ nor $\langle r\rangle$ is especially small, and the corrections can be quite large. Thus, for most of our calculations we retain the corrections to this zero-range approximation for SEQ.

Next, we evaluate the matrix element of Eq. (3.3) between shell-model states $|\psi_{Nf}\rangle$. For this we need the density matrix element

$$\langle\psi_{Nf}|\{(a^+_{j'_1}a^+_{j'_2})^{J'}(\tilde{a}_{j_2}\tilde{a}_{j_1})^J\}^{\mathscr{J}}_{\mathscr{M}}|\psi_{Ni}\rangle\equiv\sum_{MM'}\langle\mathscr{J}\mathscr{M}|J'JM'-M\rangle\langle\psi_{Nf}|(a^+_{j'_1}a^+_{j'_2})^{J'M'}(\tilde{a}_{j_2}\tilde{a}_{j_1})^{J-M}|\psi_{Ni}\rangle . \quad (3.7)$$

From Eq. (3.6) we see that the only other quantity depending on M and M' is the Clebsch-Gordon coefficient, so we use the relationship

$$\sum_{MM'}\langle J'M'|JKMM_K\rangle\langle\mathscr{J}\mathscr{M}|J'JM'-M\rangle(-)^{J+M}=\delta(\mathscr{J},K)\delta(\mathscr{M},M_K)(-)^{-\mathscr{J}-K}\left[\frac{2J'+1}{2K+1}\right]^{1/2} \quad (3.8)$$

to find our main result

$$\langle\psi_{Nf}|\hat{\mathcal{F}}^i|\psi_{Ni}\rangle=\frac{1}{2}\sum_{\{j\}}\sum_{\lambda\alpha\lambda'\beta}A_i(\lambda\alpha\lambda'\beta)\sum_{K\Lambda M_K}(-)^{-K+\Lambda-\lambda+M_K}\left[\frac{2J'+1}{(2K+1)(2\lambda+1)}\right]^{1/2}$$
$$\times f_K(\lambda\alpha\lambda'\beta;\Lambda,R)\{Y_\Lambda(\hat{R})\otimes[\mathbf{k}'\otimes\mathbf{k}]^\lambda\}^K_{-M_K}$$
$$\times\langle\psi_{Nf}|\{(a^+_{j'_1}a^+_{j'_2})^{J'}(\tilde{a}_{j_2}\tilde{a}_{j_1})^J\}^K_{M_K}|\psi_{Ni}\rangle , \quad (3.9)$$

where $\{j\}$ signifies all quantum numbers of the pair of initial and final nucleons on which the charge exchange takes place.

Similar considerations apply to the isospin quantum numbers. The simplest way to account for isospin is to note that the factor A_i in Eq. (2.26) contains a matrix element

$$\langle t=1,t_z=+1|\tau_{12}|t=1,t_z=-1\rangle=2 . \quad (3.10)$$

In the isospin analog to Eq. (3.7) the isospin of the excitation should be coupled to $T=2$, $M_T=2$ by a Clebsch-Gordan coefficient $\langle 22|1111\rangle=1$.

We are dealing with nuclei whose initial and final states have total angular momentum $I^\pi=0^+$. In this case the den-

sity matrix factor vanishes unless $K=M_K=0$ and tensors with $\lambda=1$ in Eq. (3.9) vanish when the integral over $\hat{\mathbf{R}}$ is performed. Equation (3.9) therefore simplifies to give

$$\langle \psi_{Nf}(I=0)|\hat{\mathcal{F}}_i|\psi_{Ni}(I=0)\rangle=\frac{1}{2}\sum_{\{j\}}\sum_{\lambda\alpha\lambda'\beta}\frac{A_i(\lambda\alpha\lambda'\beta)}{2\lambda+1}\sqrt{2J+1}f_0(\lambda\alpha\lambda'\beta;\lambda R)(-)^{\lambda}$$
$$\times Y_{\lambda}(\hat{\mathbf{R}})\cdot[\mathbf{k}'\otimes\mathbf{k}]^{\lambda}\langle \psi_{Nf}|\{(a^{+}_{j_1'}a^{+}_{j_2'})^J(\tilde{a}_{j_2}\tilde{a}_{j_1})^J\}^0_0|\psi_{Ni}\rangle\ , \tag{3.11}$$

where only two values of λ can occur, $\lambda=0$ and $\lambda=2$. This motivates the introduction of a scalar density $\rho_i^{(0)}(R)$ and a tensor density $\rho_i^{(2)}(R)$ defined so that

$$\langle \psi_{Nf}(I=0)|\mathcal{F}^i|\psi_{Ni}(I=0)\rangle=\mathbf{k}'\cdot\mathbf{k}\rho_i^{(0)}(R)+C_2(\hat{\mathbf{R}})\cdot[\mathbf{k}'\otimes\mathbf{k}]^2\rho_i^{(2)}(R)\ , \tag{3.12}$$

where $C_2(R)$ is a normalized spherical harmonic[17] and

$$\rho_i^{(0)}(R)=-\frac{1}{2}\sum_{\{j\}}\sqrt{2J+1}\sum_{\lambda'\alpha\beta}\frac{A_i(0,\alpha,\lambda'\beta)}{\sqrt{12\pi}}f_0(0\alpha\lambda'\beta;2,R)\langle \psi_{Nf}|\{(a^{+}_{j_1'}a^{+}_{j_2'})^J(\tilde{a}_{j_2}\tilde{a}_{j_1})^J\}^0_0|\psi_{Ni}\rangle\ , \tag{3.13}$$

$$\rho_i^{(2)}(R)=\frac{1}{2}\sum_{\{j\}}\sqrt{2J+1}\sum_{\lambda'\alpha\beta}\frac{A_i(2,\alpha,\lambda'\beta)}{\sqrt{20\pi}}f_0(2\alpha\lambda'\beta;0,R)\langle \psi_{Nf}|\{(a^{+}_{j_1'}a^{+}_{j_2'})^J(\tilde{a}_{j_2}\tilde{a}_{j_1})^J\}^0_0|\psi_{Ni}\rangle\ . \tag{3.14}$$

In evaluating Eq. (3.1) with $\langle \psi_{Nf}|D_i\delta(\mathbf{R}'-\mathbf{R})|\psi_{Ni}\rangle$ given in Eq. (3.12), we have taken the explicit factors $\mathbf{k}'$ and $\mathbf{k}'$ in Eq. (3.12) as the *relative* pion-nucleon momenta. Neglecting fermi motion in evaluating the expressions for the relative momenta, we then relate $\mathbf{k}$ to the laboratory pion momenta $\mathbf{k}_L$ by

$$\mathbf{k}=\mathbf{k}_L M_n/\sqrt{s}\ . \tag{3.15}$$

In addition to this dependence on k and k', quantities f_0 depend on these momenta through the factor $e^{i\mathbf{Q}\cdot\mathbf{r}}$ in Eq. (2.21). The simplest possible treatment of $\mathbf{k}$ would be to assume $|\mathbf{k}|=|\mathbf{k}'|=k_0\equiv$ the incident pion momentum. However, this approximation is not strictly valid because $\mathbf{k}$ and $\mathbf{k}'$ are the pion momenta *inside* the nucleus. In Appendix C we study the resulting operator distortion corrections arising from these momenta in the Eikonal approximation in conjunction with the optical potential.

IV. NUCLEAR MATRIX ELEMENTS

Nuclear structure enters through the function $f_{KM_K}(\lambda\alpha\lambda'\beta;\Lambda,R)$ in Eq. (3.5) and through the density matrix elements in Eq. (3.7). The density matrix elements must be taken from a separate nuclear-structure calculation, and we assume that this array of numbers is the same as in Ref. 6. In this section we show how to calculate the nuclear matrix elements in a single-particle basis and give numerical results for some of the simple transitions.

One must use nuclear wave functions with realistic tails for the purpose of studying reactions with strongly absorbed projectiles such as pions. Evaluation of radial integrals such as those that appear in Eq. (3.5) is simplified by using a harmonic-oscillator basis, and we next give expressions that are obtained using these radial wave functions. For heavy nuclei, one may utilize the formulae of this section, but it must be recognized that because harmonic-oscillator wave functions are not satisfactory as single-particle orbits, the more realistic Woods-Saxon or Hartree-Fock states must be expanded first in terms of them.

Beginning with Eqs. (3.5) and (3.6) we transform from j-j coupling to L-S coupling. Next, we use the Moskinsky coefficients[24] $\langle n_1l_1n_2l_2L|\tilde{N}\tilde{L}\tilde{n}\tilde{l}L\rangle$ to express the wave functions in terms of relative and center-of-mass variables. So we use

$$|(j_1j_2)JM\rangle=\sum_{\substack{LS\\ \tilde{j}}}\sum_{\substack{\tilde{N}\tilde{L}\\ \tilde{n}\tilde{l}}}|\tilde{N}\tilde{L},(\tilde{n}\tilde{l}S)\tilde{j};JM\rangle\langle LS\tilde{N}\tilde{L}\tilde{n}\tilde{l}\tilde{j}|(j_1j_2)J\rangle\ , \tag{4.1}$$

where

$$\langle LS\tilde{N}\tilde{L}\tilde{n}\tilde{l}\tilde{j}|(j_1j_2)J\rangle\equiv\sqrt{(2L+1)(2S+1)(2j_1+1)(2j_2+1)}\begin{Bmatrix} l_1 & l_2 & L\\ \frac{1}{2} & \frac{1}{2} & S\\ j_1 & j_2 & J\end{Bmatrix}$$
$$\times\sqrt{(2L+1)(2\tilde{j}+1)}(-)^{\tilde{L}+\tilde{l}+J+S}\begin{Bmatrix}\tilde{L} & \tilde{l} & L\\ S & J & \tilde{j}\end{Bmatrix}\langle n_1l_1n_2l_2L|\tilde{N}\tilde{L}\tilde{n}\tilde{l}L\rangle\ . \tag{4.2}$$

We then need the matrix elements of Eq. (3.5) [or (B7) when finite range corrections are added]. For example, from Eq. (3.5) we have to evaluate

$$\langle \tilde{N}\tilde{L},(\tilde{n}\tilde{l}S)\tilde{j};J\|d_i(\alpha,\mathbf{r}')\frac{\delta(R-R')}{R^2}[Y_\Lambda(\hat{\mathbf{R}}')\otimes[Y_\alpha(\hat{\mathbf{r}}')\otimes S_\beta^{\lambda'}(\sigma_1,\sigma_2)]^\lambda]^K_{M_K}\|\tilde{N}'\tilde{L}',(\tilde{n}'\tilde{l}'S'),\tilde{j}';J'\rangle \ . \tag{4.3}$$

Because we retain only the $l=0$ piece of $e^{i\mathbf{Q}\cdot\mathbf{r}}$, we may use the reduction formula (Appendix VI of Ref. 17) twice to obtain

$$\text{Eq.}(4.3)=[(2J'+1)(2K+1)(2\tilde{L}+1)(2\tilde{j}+1)(2\tilde{j}'+1)(2\lambda+1)(2\tilde{l}+1)(2S+1)]^{1/2}\begin{Bmatrix} J & J' & K \\ \tilde{L} & \tilde{L}' & \Lambda \\ \tilde{j} & \tilde{j}' & \lambda \end{Bmatrix}$$

$$\times\begin{Bmatrix} \tilde{j} & \tilde{j}' & \lambda \\ \tilde{l} & \tilde{l}' & \alpha \\ S & S' & \lambda' \end{Bmatrix}\langle\tilde{L}\|Y_\Lambda(\hat{\mathbf{R}}')\|\tilde{L}'\rangle\langle\tilde{n}\tilde{l}\|Y_\alpha(\hat{\mathbf{r}}')d_i(\alpha,\mathbf{r}')\|\tilde{n}'\tilde{l}'\rangle\langle(\tfrac{1}{2}\tfrac{1}{2})S\|S_\beta^{\lambda'}(\sigma_1,\sigma_2)\|(\tfrac{1}{2}\tfrac{1}{2})S'\rangle R_{\tilde{N}\tilde{L}}(R)R_{\tilde{N}'\tilde{L}'}(R) \ . \tag{4.4}$$

Expressions for the reduced matrix elements of $Y_\Lambda(\hat{\mathbf{R}})$ and $S_\beta^{\lambda'}$ may be found in Ref. 17. In Eq. (4.4), $R_{\tilde{N}\tilde{L}}(R)$ is the radial harmonic-oscillator wave function, and $\langle\tilde{n}\tilde{l}\|Y_\alpha d_i\|\tilde{n}'\tilde{l}'\rangle$ is defined by

$$i\frac{\bar{k}^3v^2(\bar{k})}{m_\pi^2}\int d^3r' Y^*_{\tilde{l}\tilde{m}}(\hat{\mathbf{r}}')R_{\tilde{n}\tilde{l}}(r')Y_{\alpha m}(\hat{\mathbf{r}}')H_\alpha(\bar{k},r')\Gamma(r')Y_{\tilde{l}'\tilde{m}'}(\hat{\mathbf{r}}')R_{\tilde{n}'\tilde{l}'}(r')e^{+i\mathbf{Q}\cdot\mathbf{r}'}\equiv\langle\tilde{n}\tilde{l}\|Y_\alpha d_i\|\tilde{n}'\tilde{l}'\rangle\langle\tilde{l}\tilde{m}\,|\tilde{l}'\alpha\tilde{m}'m\rangle \ . \tag{4.5}$$

Since the $l=0$ piece of $e^{i\mathbf{Q}\cdot\mathbf{r}}$ is $j_0(Qr)$, we find

$$\langle\tilde{n}\tilde{l}\|Y_\alpha d_i\|\tilde{n}'\tilde{l}'\rangle=i\frac{\bar{k}^3v^2(\bar{k})}{m_\pi^3}\langle\tilde{l}\|Y_\alpha\|\tilde{l}'\rangle\int_0^\infty r'^2dr'R_{\tilde{n}\tilde{l}}(r')R_{\tilde{n}'\tilde{l}'}(r')H_\alpha(\bar{k},r')j_0(Qr')\Gamma(r') \ . \tag{4.6}$$

We are now ready to show numerical results. First, however, let us consider the choice of $\bar{R}$ in Eq. (2.22). To determine it we have normalized our DWIA calculation to the results of a PIESDEX coupled-channel calculation[22] for a transition of two neutrons in $s_{1/2}$ orbitals to two protons in the $s_{1/2}$ orbitals. For the DWIA calculations, we eliminated the ρ meson and the short-range correlation function, and we set $\Lambda_\pi\to\infty$. We also eliminated the spin-dependent tensors to ensure that the only intermediate analog-state transitions would contribute to the double charge exchange, which is a restriction built into the coupled-channel calculation. We confirmed that the two calculations gave the same answer when the distorting interaction was turned off. With $\bar{R}=2.8$ fm, the DWIA and coupled-channel results agree at 165 MeV when the distortions are turned back on. We have used this value of $\bar{R}$ for all our SEQ calculations.

The theory described above has been put together in the computer program SHIN. For our first results, consider the relative contributions of the tensors that contribute to Eq. (3.12) for SEQ in the zero-range approximation, i.e., without the corrections of Appendix B, and for DINT. For these calculations we have used the values[6]

$$\Lambda_\pi=5.5\ \text{fm}^{-1}$$
$$\Lambda_\rho=6.41\ \text{fm}^{-1} \tag{4.7}$$

which normalizes DINT to the forward nonanalog DCX cross section at $T_\pi=165$ MeV on ^{16}O. Typical results are given in Fig. 8. The short dashed curves correspond to DINT and the dotted curves correspond to SEQ. It is seen that the tensors 1, 2, and 6 dominate. The tensors 3, 4, 5, and 7 are the ones that contribute to $\rho^{(2)}$ in Eq. (3.13) and the fact that they are small makes a considerable simplification in the calculation. The DWF contri-

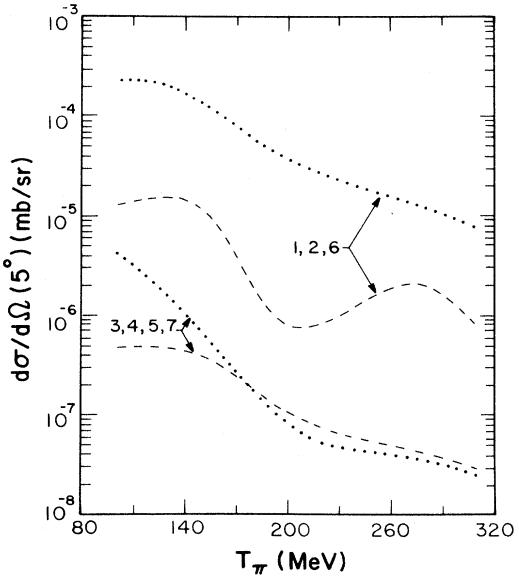

FIG. 8. Showing the relative importance of the tensors (1, 2, and 6) and (3, 4, 5, and 7) of Table I. The dashed curve is DINT and the dotted curve is SEQ. The calculation corresponds to the $d^2_{5/2}\to d^2_{5/2}$ in oxygen. Tensors (3, 4, 5, and 7) are comparably small for all other transitions.

TABLE III. $(d\sigma/d\Omega)$ (5°) (μb/sr) at $T_\pi = 164$ MeV for different single-particle orbits $(nj)^2$ coupled to $J^\pi = 0^+$, corresponding to the DINT process. The form factors have been chosen as in Eq. (4.7).

$(nj)_i/(nj)_f$	$1p_{3/2}$	$1p_{1/2}$	$1d_{5/2}$	$2s_{1/2}$	$1d_{3/2}$
$1p_{3/2}$	0.135	0.301	0.077	0.044	0.394
$1p_{1/2}$	0.301	0.002	0.378	0.022	0.009
$1d_{5/2}$	0.077	0.378	0.034	0.114	1.099
$2s_{1/2}$	0.044	0.022	0.144	0.128	0.076
$1d_{3/2}$	0.394	0.009	1.099	0.076	0.078

bution of Figs. 1(b) and 1(c) were shown to be negligibly small at resonance in Ref. 4, and we therefore show no numerical results for these here. They are suppressed because the "large" tensors 1, 2, and 6 do not contribute (see Table I) and because one of the Δ_{33} in Figs. 1(b) and 1(c) is off shell, suppressing its contribution relative to Figs. 1(a) and 1(d).

Consider next the relative sizes of the contributions of various transitions to the DCX cross sections. For these calculations and those in the remainder of the paper, we include the finite range corrections to DINT and SEQ, which are specified in Appendix B, Eq. (B8). Table III shows the 5° cross section for the DINT process. Note that for given l, l', the spin-flip cross sections

$$d\sigma/d\Omega(j = l \pm \tfrac{1}{2} \rightarrow j' = l' \mp \tfrac{1}{2})$$

are all larger than the non-spin-flip ones

$$d\sigma/d\Omega(j = l \pm \tfrac{1}{2} \rightarrow j' = l' \pm \tfrac{1}{2}) .$$

Corresponding results for SEQ are shown in Table IV. In contrast to DINT, the non-spin-flip transitions tend to be larger than the spin-flip transitions. Thus, nuclear structure enters quite differently into DINT and SEQ. Displayed otherwise, the ratio of SEQ/DINT tends to break down into three groups, with the largest ratio ($\gtrsim 3$) being for non-spin-flip transitions, the intermediate ratio ($\simeq 1.0$) corresponding to transitions with the $2s_{1/2}$ and the smallest ratio ($\lesssim 0.3$) corresponding to spin-flip transitions. This characterization is subject to the caveat discussed in Sec. III, that our average treatment of distortions on the intermediate pion in SEQ presumably artificially enhances the matrix elements for $l' \neq l$ in Table IV.

In Refs. 4 and 6 it was stressed that the cross sections are very sensitive to the form-factor cutoffs Λ_π and Λ_ρ, and we next show the dependences of the cross sections on these quantities. A contour plot of $d\sigma/d\Omega(5°)$ at $T_\pi = 164$ MeV for ^{16}O is shown in Fig. 9 for the DINT process. The calculation is made for the transition $p^2_{1/2} \rightarrow d^2_{5/2}$, which is one of the larger matrix elements in Table III. For a reasonable range of Λ_π ($\sim 5-6$ fm^{-1}), $d\sigma/d\Omega(5°)$ increases monotonically with Λ_ρ for $\Lambda_\rho > 5$ fm^{-1}. The details depend sensitively on the pair distribution function $\Gamma(r)$, which cuts out the pieces of the ρ-meson-exchange force proportional to $\delta(r)$ that arises as $\Lambda_\rho \rightarrow \infty$. The sign of the δ-function force is opposite to the familiar Yukawa piece proportional to $e^{-m_\rho r}/r$. A contour plot for SEQ is shown in Fig. 10. Here, we give results for $d^2_{5/2} \rightarrow d^2_{5/2}$, the dominant transition in Table IV. For $\Lambda_\pi = 5-6$ fm^{-1}, the cross section $d\sigma/d\Omega(5°)$ is insensitive to Λ_ρ as long as it is not too large ($\Lambda_\rho < 7$ fm^{-1}). The sensitivity to Λ_π and Λ_ρ is reduced in comparison to DINT because the exchanged meson now carries the energy and momentum.

Finally, in this section we want to examine the interplay between the short-range correlations and pionic form factor for simple configurations. We should stress in advance that we have assumed that the mesons propagate according to the Klein-Gordon equation, and that a linearized meson propagator such as that used in Ref. 7 may lead to different results. Table V shows results for SEQ for various choices of Λ_π (we omit the ρ meson), with and without the correlation function. Table VI shows a similar calculation for DINT. Note that the calculation is fairly stable for variations of Λ_π about the value in Eq. (4.7) but that a rather strong sensitivity to the correlation function is found for DINT.

V. NUMERICAL RESULTS WITH REALISTIC WAVE FUNCTIONS

In Sec. IV we showed the sensitivity of DINT and SEQ to the underlying dynamical model: choice of form factor, short-range correlation function, and nuclear struc-

TABLE IV. $(d\sigma/d\Omega)$ (5°) (μb/sr) at $T_\pi = 164$ MeV for different single-particle orbits $(nj)^2$ coupled to $J^\pi = 0^+$, corresponding to the SEQ process. The form factors have been chosen as in Eq. (4.7).

$(nj)_i/(nj)_f$	$1p_{3/2}$	$1p_{1/2}$	$1d_{5/2}$	$2s_{1/2}$	$1d_{3/2}$
$1p_{3/2}$	0.395	0.087	0.407	0.060	0.105
$1p_{1/2}$	0.087	0.192	0.067	0.030	0.255
$1d_{5/2}$	0.407	0.067	0.912	0.148	0.129
$2s_{1/2}$	0.060	0.030	0.148	0.169	0.098
$1d_{3/2}$	0.105	0.255	0.129	0.098	0.745

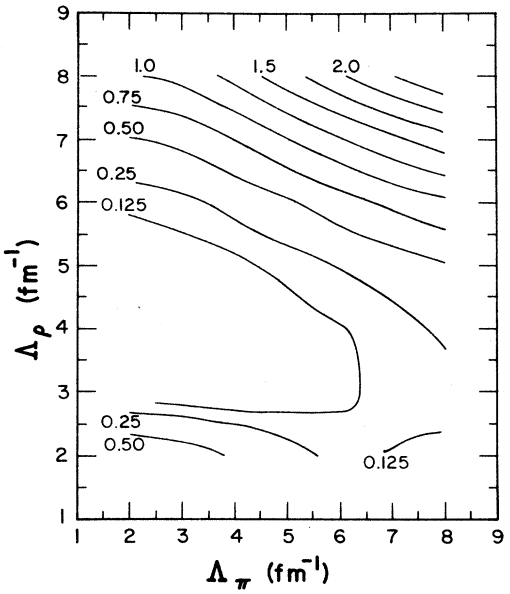

FIG. 9. Contour plot of $d\sigma/d\Omega$ (5°) at $T_\pi = 165$ MeV for DINT as a function of the pion and ρ-meson from factors Λ_π and Λ_ρ. The $\rho^2_{1/2} \rightarrow d^2_{5/2}$ transition amplitude is calculated in ^{16}O. The numbers on the curves are the cross sections in μb/sr.

ture, for particular shell-model configurations. We will continue this examination in the current section using realistic wave functions for ^{18}O and ^{16}O.

First, let us consider how important the background

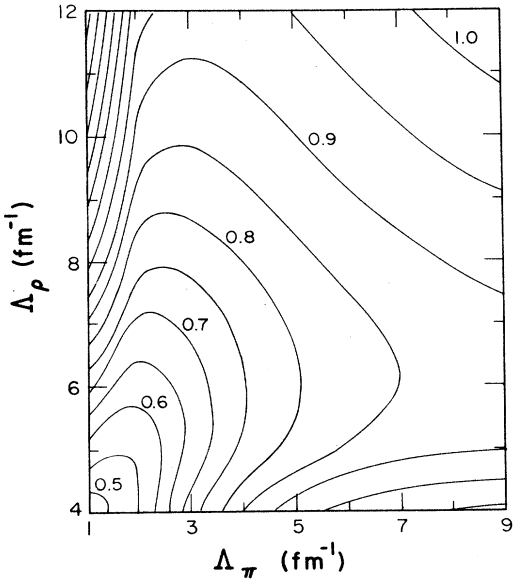

FIG. 10. Contour plot of $d\sigma/d\Omega$ (5°) at $T_\pi = 165$ MeV for SEQ as a function of the pion and ρ-meson form factors Λ_π and Λ_ρ. The $d^2_{5/2} \rightarrow d^2_{5/2}$ transition amplitude is calculated in ^{18}O. The numbers on the curves are cross sections in μb/sr.

TABLE V. $(d\sigma/d\Omega)$ (5°) (μb/sr) for SEQ (^{18}O) as a function of Λ_π at 160 MeV, showing sensitivity to the correlation function. We have omitted the ρ meson and we look at $d^2 \rightarrow d^2$ transitions only.

Λ_π (fm^{-1})	With correlation function	Without correlation function
1.5	0.557	0.573
2.5	0.805	0.855
3.5	0.998	1.10
4.5	1.12	1.28
6.5	1.21	1.48
8.5	1.23	1.58
20.0	1.21	1.73

(non-Δ_{33}) pieces of the pion-nucleon scattering amplitudes are for the calculation of SEQ. Our formulation in Sec. II is built about the Δ_{33} resonance, and to properly take into account sequential DCX including the s-wave pion-nucleon scattering amplitude, we should accordingly generalize our results. This is a difficult calculation, but the appropriate extension will be discussed in a forthcoming publication.[18] We can, however, make an approximation evaluation by replacing the resonance in Eq. (2.10) by

$$e^{i\delta_{33}}\sin\delta_{33} = \frac{-W/2}{\sqrt{s} - M_\Delta + iW/2} \rightarrow f_{\rm CEX} \tag{5.1}$$

where $f_{\rm CEX}$ is the sum over all appropriately normalized s- and p-wave isovector amplitudes. We show in Fig. 11 a comparison between the results of the zero-ranged ($\Lambda_\pi \rightarrow \infty$) coupled-channel model of Ref. 22 and the calculation of the DWIA calculation using Eq. (3.1) in the special case of no ρ meson, $\Gamma(r) = 1$, and $\Lambda_\pi \rightarrow \infty$. The transition density corresponds to neutrons and protons in a pure $d^2_{5/2}$ configuration, calculated from Hartree-Fock with the Skyrme III effective interaction in the coupled-channel case and with harmonic-oscillator wave functions in the DWIA. Note that the cross section of the DWIA delta-only result (dashed curve) is peaked, decreasing for energies above about 110 MeV. This behav-

TABLE VI. $d\sigma/d\Omega$ (5°) (μb/sr) for DINT (^{18}O) as a function of Λ_π at 160 MeV, showing sensitivity to the correlation function. We have omitted the ρ meson and we look at $d^2 \rightarrow d^2$ transitions only.

Λ_π (fm^{-1})	With correlation function	Without correlation function
1.5	0.208	0.229
2.5	1.03	1.36
3.5	1.41	2.42
4.5	1.32	3.13
6.5	0.824	3.87
8.5	0.467	4.20
20.0	0.049	4.71

ior reflects the interplay between the two strongly energy-dependent delta propagators in Fig. 1(d), and the distortions of the initial and final pion waves. On the other hand, the coupled-channel result (dot-dashed curve) monotonically increases from 100 MeV. The difference between the solid and dashed curves arises from the interference between the s-wave and the p-wave isovector pion-nucleon scattering amplitudes, which is destructive below resonance and constructive above. This is confirmed by coupled-channel result (dot-dashed curve). Thus, the s-wave pion-nucleon scattering amplitude is very important in DCX. The remaining calculations of SEQ will include the s-wave amplitude in this approximate form.

Note that the DWIA solid curve in Fig. 11 lies above the coupled-channel result by about a factor of 2 or more. The main distinction between the coupled-channel result of Ref. 22 and our DWIA calculation of Fig. 1(d) is that the latter includes all intermediate states allowed by closure and by the choice of the wave function of the initial and final state, whereas the former includes only the isobaric analog state as an intermediate state. The influence of nonanalog intermediate states in DCX is known to be important[7] and presumably accounts for part of the difference. However, because of the limitations of our treatment of distortions and the s-wave pion-nucleon interaction, the magnitude of this difference is probably not reliably calculated.

The nuclear structure of ^{16}O and ^{18}O is known to be complex. Experimentally, this feature appears as the existence of a low-lying 0^+ state in ^{16}O and a significant amount of $M1$ strength around $E_x=15-20$ MeV. The shell-model calculations for these nuclei are customarily performed in the ZBW space[25] ($p_{1/2}$, $d_{5/2}$, and $s_{1/2}$). The resulting transition amplitudes for DCX are provided as

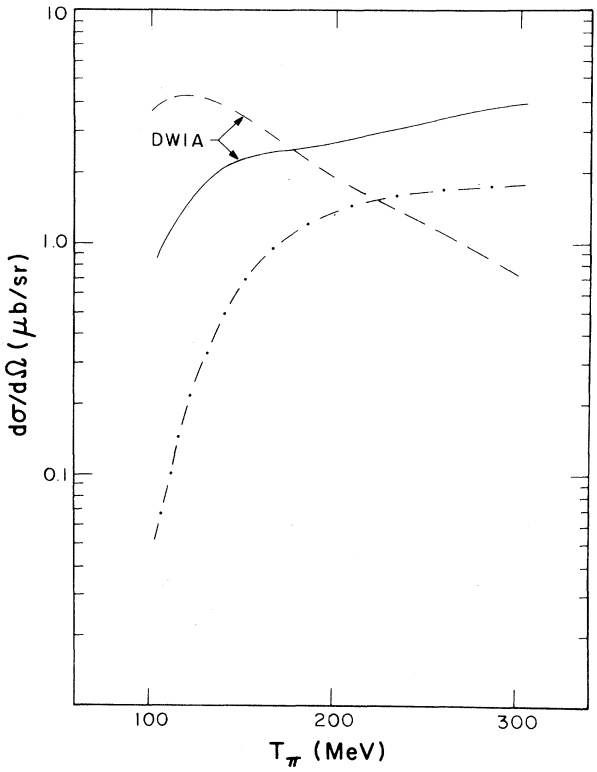

FIG. 11. Comparison of the DWIA calculation to coupled-channel (dot-dashed) calculation of SEQ taken from Ref. 22. The solid curve is the DWIA evaluated with s- and p-wave pion-nucleon scattering amplitudes and the dashed curve includes only the deltas as in Fig. 1(d).

$$-\tfrac{1}{2}\langle {}^{16}\mathrm{N}\|\{(a^+a^+)^{0,1}(\tilde{a}\tilde{a})^{0,1}\}^{0,2}\|{}^{16}\mathrm{O}\rangle = 0.2(p_{1/2}^2\to p_{1/2}^2) - 0.777(p_{1/2}^2\to d_{5/2}^2) - 0.616(p_{1/2}^2\to s^2) + 0.248(d_{5/2}^2\to d_{5/2}^2) + 0.272(d_{5/2}^2\to s_{1/2}^2) + 0.045(s_{1/2}^2\to s_{1/2}^2) \quad (5.2)$$

and

$$-\tfrac{1}{2}\langle {}^{18}\mathrm{N}\|\{(a^+a^+)^{0,1}(\tilde{a}\tilde{a})^{0,1}\}^{0,2}\|{}^{18}\mathrm{O}\rangle = 0.235(p_{1/2}^2\to p_{1/2}^2) - 0.78(p_{1/2}^2\to d_{5/2}^2) - 0.414(p_{1/2}^2\to s_{1/2}^2) + 0.780(d_{5/2}^2\to d_{5/2}^2) + 0.698(d_{5/2}^2\to s_{1/2}^2) + 0.143(s_{1/2}^2\to s_{1/2}^2)\,, \quad (5.3)$$

where the left-hand side is the reduced matrix element (reduced in total angular momentum only, with the convention of Ref. 17) of the operator in Eq. (3.6). The right-hand sides of Eqs. (5.2) and (5.3) were obtained from Ref. 26 and are the same as the TBTD matrix elements[27] of the code OXBASH.[28] The superscripts 0,1 in Eqs. (5.2) and (5.3) refer to the total spin and isospin of the pair, and the superscripts 0,2 refer to the transferred spin and isospin of the two-particle, two-hole excitation. Symmetry makes the coefficients corresponding to neutron $(nlj)^2\to$proton$(n'l'j')^2$ the same as neutron $(n'l'j')^2\to$proton$(nlj)^2$, allowing us to simplify writing the matrix elements in Eqs. (5.2) and (5.3). All $0^+\to 0^+$ pair configurations existing in the model space are shown here, but OXBASH also calculates $J_{pp}=J_{nn}\neq 0$ components (two protons and two neutrons couple first to J_{pp} and J_{nn} and the couple to $\mathcal{J}=0$), which have a small effect on the cross section[29] for these nuclei and have not been included.

The following calculations all use the wave functions in Eqs. (5.2) and (5.3), the form factor cutoffs of Eq. (4.7), and the short-range correlation function of Eq. (2.27). We first show, in Fig. 12, the sensitivity of DINT and SEQ to the ρ meson. One can see already from Figs. 9 and 10 that this sensitivity is an intricate function of the form factors of the π and ρ meson. What is not apparent from these figures is that the interference between the two contributions can be either constructive or destructive. With our particular choice of form factor, the ρ meson interfaces destructively with the π meson. For

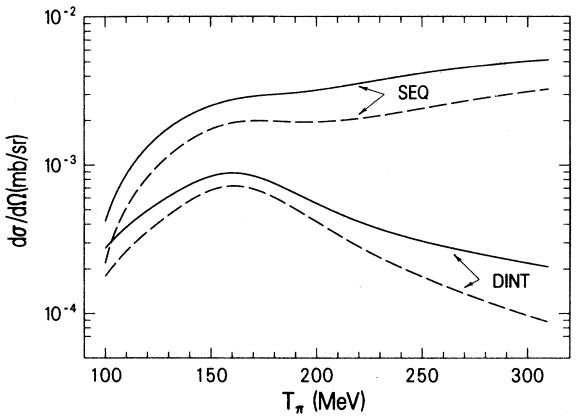

FIG. 12. Showing the sensitivity to the ρ meson for DINT and SEQ. Calculations are shown for ^{18}O using the wave function in Eq. (5.3) and form factors in Eq. (4.7). The solid curves include the ρ meson.

DINT, the ρ-meson contribution to the cross section alone is about a factor of four greater than that of the π meson alone, whereas for SEQ the relative size of the ρ is much less. Next, consider the sensitivity to short-range correlations, which is illustrated in Fig. 13. For DINT, the removal of $\Gamma(r)$ results in an increase of the cross section by more than a factor of 10. In contrast to DINT, the SEQ cross sections increase only by about a factor of three, reflecting the fact that this process picks up dominant contributions from π exchange at rather long range. The increased sensitivity in comparison to the results in Tables V and VI arises in part from our inclusion of the ρ meson here. The ρ meson is much more important than one might guess from Fig. 12 because of large contributions that arise at small r.

We shall next show the energy dependence of each single-particle configuration of the transition. The DCX cross sections at $\theta_{CM}=5°$ for ^{16}O with DINT are shown in Fig. 14. Most of the configurations for DINT provide an energy dependence with a bump around 165 MeV, except for the $p^2_{1/2}\rightarrow p^2_{1/2}$ transition. The odd feature of the $p^2_{1/2}\rightarrow p^2_{1/2}$ transition is caused by the effective form factor $\rho^{(0)}(r)$ [Eq. (3.13)] having a node outside of the nuclear radius. Thus, a delicate cancellation is involved, and the net result depends on the extent of pion distortions. The $p^2_{1/2}\rightarrow d^2_{5/2}$ transition far dominates (see also Table III) the rest of the components and reproduces the experimental energy dependence. The full cross section is shown by the solid line. The results for SEQ on ^{18}O is shown in Fig. 15. Because the $d^2_{5/2}\rightarrow d^2_{5/2}$ transition is heavily weighted in the wave function of Eq. (5.3), we find that the cross section is dominated by this one transition.

Finally, we want to show the relative sizes of SEQ and DINT for ^{18}O. We will use form factors and coupling constants for DINT which describe the nonanalog data, and for SEQ we take the same calculation already described in Fig. 15. The results are shown in Fig. 16. One sees that DINT is comparable in size to the data at resonance and could be significant in its interpretation. It is also apparent from Fig. 16 that DINT and SEQ are approximately out of phase by about $\pi/2$. To reproduce the structure which is seen in the excitation function and the anomalous angular distribution at 165 MeV in ^{18}O, the two amplitudes should rather be out of phase by about π at this energy.

For the planning of future activity on this problem, one should keep in mind the phenomenological result[30] that large second-order medium renormalizations to the SCX amplitudes are believed to occur at resonance, and that these would change the phase (and magnitude) of SEQ double charge exchange there. These second-order

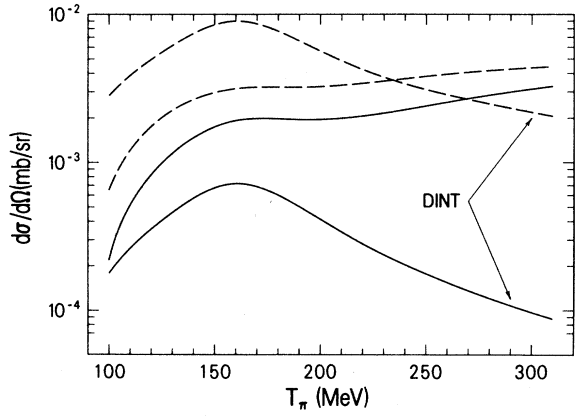

FIG. 13. Showing the sensitivity to the short-range correlation function for DINT and SEQ. Calculations are shown for ^{18}O using the wave function in Eq. (5.3) and the form factors in Eq. (4.7). The solid curves include the correlation function.

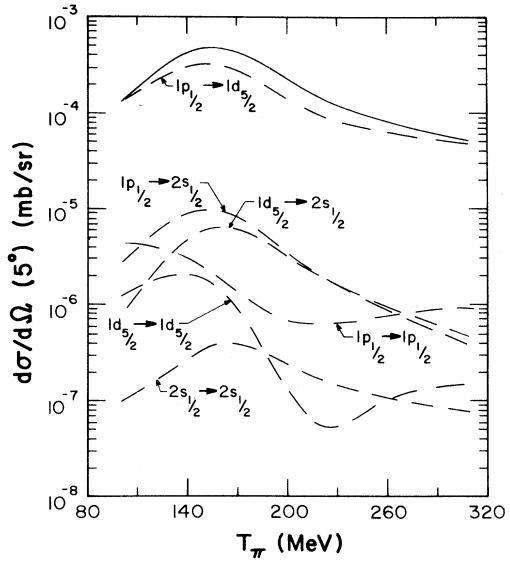

FIG. 14. Contributions to $d\sigma/d\Omega$ (5°) arising from individual orbitals for the DINT process on ^{16}O. The solid line is the net cross section. The individual components are indicated on the figure.

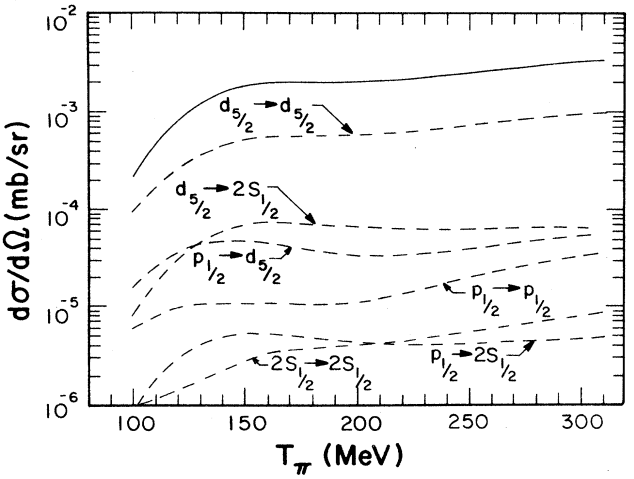

FIG. 15. Contributions to $d\sigma/d\Omega$ (5°) arising from individual orbitals for the SEQ process on ^{18}O. The solid line is the net cross section. The individual components are indicated on the figure.

corrections are poorly understood theoretically and have not been included in our calculation. As discussed in the introduction, there are also additional pieces to $V_{N\Delta}$ arising from the exchange of two pions, and these could alter the phase of $V_{N\Delta}$. It is also possible that improving the treatment of the π^0 distortions given in Eq. (2.22) would change the relative phase.

One clearly sees in Fig. 16 that DINT and SEQ have a different energy dependence. The SEQ mechanism tends to rise monotonically from about 100 MeV, whereas DINT has a pronounced peak at about 150 MeV. This difference is due to the fact, already described, that the s waves interfere with the p waves destructively below resonance and constructively above resonance. This occurs in SEQ but not in DINT, giving rise to some possibility that the two mechanisms can be distinguished in the experimental data.

Because of our belief that the contribution of SEQ to the cross section is overestimated by our DWIA methods, especially for $l \neq l'$ transitions, we do not show cross sections for SEQ in ^{16}O, where several of the important transitions seen in Eq. (5.2) have this character. We have found, however, that if we simply delete these orbital-angular-momentum-changing transitions, then SEQ is relatively flat at about 110 μb between 150- and 300-MeV kinetic energy. This is about a factor of 5 below the nonanalog data at resonance and comparable to it at 300 MeV. Such a strong suppression of SEQ for nonanalog transitions was found in a coupled-channel calculation in Ref. 31.

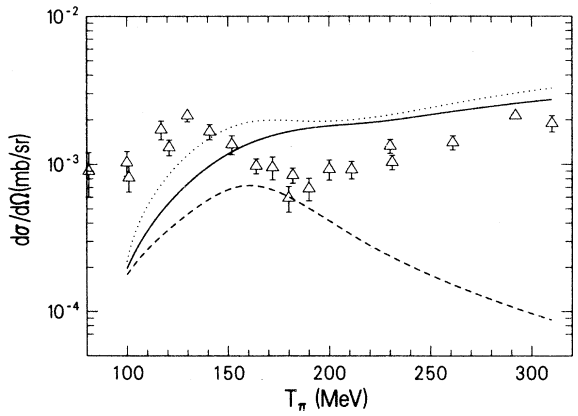

FIG. 16. $d\sigma/d\Omega$ (5°) on ^{18}O. The solid line is the sum of DINT and SEQ. The dotted curve is SEQ and the dash, DINT.

VI. DISCUSSION AND CONCLUSIONS

The delta-nucleon interaction $V_{N\Delta}$ is an important quantity in medium energy and nuclear physics, and nonanalog pion double charge exchange has been found[6] to be one reaction that is especially sensitive to this quantity. Our main tasks in this paper have been to study in detail the contribution of $V_{N\Delta}$, which we have called DINT in this context, to nonanalog and analog pion double charge exchange, and, in addition, to show numerical results explicating its sensitivity to the rho meson, short-range correlations, and the nuclear wave function. We use here a coordinate-space approach, in which a detailed tensoral decomposition of DINT along with standard angular-momentum algebra can be used to bring together the reaction mechanism and nuclear shell-model wave functions. This is the procedure followed in our earlier work,[4–6] in which the details were only sketched. Checks have been made in the plane-wave limit by comparing to independent coupled-channel calculations for SEQ and momentum-space evaluations[8] of DINT. We have used the distorted-wave approximation for obtaining our numerical results, and the answers found here are completely consistent with the earlier work.[4–6]

We found that the sequential reaction mechanism, SEQ, could be evaluated approximately using an analogous tensoral decomposition, and so we have looked at similar model sensitivity in this case also, when we believed that our approximations justified it. For reasons detailed in the body of the paper, the absolute magnitude of the SEQ process, especially for the contributions of transitions between orbits of different orbital angular momenta, is not as accurately calculated as for DINT, but we have gained insight into both reaction mechanisms by making the comparison between the two. We found that the sensitivity to the ρ meson and to short-range correlations was less pronounced for SEQ than for DINT. We also found that DINT is sensitive mainly to transitions in which the spin flips, where SEQ is sensitive mainly to those in which the spin does not flip. If the orbit-changing transitions are completely suppressed in SEQ, which we expect to be approximately the case on theoretical grounds, we estimate that SEQ is about a factor of 5 smaller than DINT in ^{16}O at resonance.

It is, of course, important to be aware of signatures that might distinguish the DINT and SEQ reaction mechanisms. In addition to the different sensitivity to the spin character of the transitions involved, we have

found that the energy dependence of the two mechanisms differs. In the region of pion kinetic energy between 100 and 300 MeV, DINT has a peaked energy dependence, whereas SEQ tends to rise monotonically. This difference is caused by the pion-nucleon isovector s-wave amplitude, which contributes to SEQ but not DINT. As we have indicated in an earlier publication,[6] the nonanalog experimental data are consistent with not only the energy dependence, but also the angular distributions and A dependence of DINT.

In earlier work[4,8] it was shown that DINT might play an important role in analog transitions, but a definite statement about the size of its contribution in these transitions depended upon knowing the $\pi\Delta\Delta$ and $\rho\Delta\Delta$ form factors, which cannot be determined from theoretical considerations at the present time. We showed in this paper that when these form factors are determined by a fit of the theory to the nonanalog data,[6] DINT is comparable in size to the analog data in ^{18}O at resonance and is apparently out of phase by $\pi/2$ with the lowest-order SEQ calculation. However, as we have indicated, the phase may be changed by the addition of two-meson-exchange terms to DINT or by medium modifications to the isovector single-charge-exchange amplitudes in SEQ.

Although there are many outstanding problems remaining in understanding pion double charge exchange in the resonance region, we believe, based on the results in this paper, that a combined understanding of analog and nonanalog DCX in the region of the Δ_{33} resonance is likely to be an important source of information about the delta-nucleon interaction.

ACKNOWLEDGMENTS

We thank T. Erikson, H. T. Fortune, E. Oset, and D. Strottman for stimulating discussions. We also express appreciation to M. Burlein for help with some of the numerical calculations.

APPENDIX A: TWO-BODY OPERATOR AND ANTISYMMETRIZATION

The counting of the diagrams in DCX requires some care. Because the N and Δ are distinguishable, the statistical factors that enter for $N\Delta$ scattering are different from what one might expect from experience in NN scattering. As an example, we take the DINT process. First, we construct the two-body operator of Eq. (2.20), $\theta(1,2)=\theta_{12}+\theta_{21}$, where the Δ's are excited for particle 1 in one process and in the other for particle 2 as shown in Fig. 5.

The resulting two-body operator is symmetric under the interchange of the particles 1 and 2. For pure NN scattering there would be just one term because that alone is symmetric under interchange of 1 and 2. Next, sandwich this operator by fully antisymmetrized wave functions from the left and from the right. For example, if we have scattering from two particles in levels α,β then

$$M=\langle \frac{1}{\sqrt{2}}[\psi_\alpha(1)\psi_\beta(2)-\psi_\beta(1)\psi_\alpha(2)]|\theta(1,2)|\frac{1}{\sqrt{2}}[\psi_{\alpha'}(1)\psi_{\beta'}(2)-\psi_{\beta'}(1)\psi_{\alpha'}(2)]\rangle \ . \tag{A1}$$

This is precisely equal to

$$M=\langle \psi_\alpha(1)\psi_\beta(2)-\psi_\beta(1)\psi_\alpha(2)|\theta(1,2)|\psi_{\alpha'}(1)\psi_{\beta'}(2)\rangle \ . \tag{A2}$$

Graphically, it corresponds to Fig. 6. We see that each topologically distinct process gets counted with overall weight of unity, which is generally expected for quantum mechanical amplitudes.

APPENDIX B: FINITE RANGE CORRECTIONS

In Sec. IV we showed how to evaluate nuclear matrix elements assuming that Qr remains small enough to permit replacing $e^{i\mathbf{Q}\cdot\mathbf{r}}$ in Eq. (4.5) by $j_0(Qr)$. In this appendix we want to indicate how to evaluate corrections to this approximation. Begin with Eq. (2.24) written out as

$$D_i(\mathbf{k}',\mathbf{k};\mathbf{r})=\sum_{\substack{\lambda\alpha\lambda'\\ \beta}} A_i(\lambda\alpha\lambda'\beta)\bar{d}_i(\alpha,\mathbf{r})e^{i\mathbf{Q}\cdot\mathbf{r}}[[\mathbf{k}\otimes\mathbf{k}']^\lambda,[Y_\alpha(\hat{\mathbf{r}})\otimes S_\beta^{\lambda'}]^\lambda]^0 \ , \tag{B1}$$

where $\bar{d}_i$ differs from d_i in Eq. (2.25) by the factor $e^{i\mathbf{Q}\cdot\mathbf{r}}$, now written explicitly in Eq. (B1).

We begin by expanding $e^{i\mathbf{Q}\cdot\mathbf{r}}$

$$e^{i\mathbf{Q}\cdot\mathbf{r}}=4\pi\sum_\nu i^\nu j_\nu(Qr)Y_\nu^*(\hat{\mathbf{Q}})\cdot Y_\nu(\hat{\mathbf{r}}) \tag{B2}$$

and combining $Y_\nu(\hat{\mathbf{r}})$ in Eq. (B2) with $Y_\alpha(\hat{\mathbf{r}})$ in Eq. (B1). After a series of recoupling operations we find

$$D_i(\mathbf{k}',\mathbf{k};\mathbf{r})=\sum_{\lambda\alpha\lambda'\beta}\sum_{\nu\mathcal{K}f} A_i(\lambda\alpha\lambda'\beta)\bar{d}_i(\alpha,\mathbf{r})i^\nu j_\nu(Qr)(-)^{\alpha+\lambda+\lambda'+\mathcal{K}}\sqrt{(2\nu+1)(2f+1)(2\mathcal{K}+1)(2\alpha+1)}$$
$$\times\begin{bmatrix}\nu & \alpha & \mathcal{K}\\ 0 & 0 & 0\end{bmatrix}\begin{Bmatrix}\nu & \mathcal{K} & \alpha\\ \lambda' & \lambda & f\end{Bmatrix}\{[[\mathbf{k}\otimes\mathbf{k}']^\lambda\otimes Y_\nu(\hat{\mathbf{Q}})]^f\otimes[Y_{\mathcal{K}}(\hat{\mathbf{r}})\otimes S_\beta^{\lambda'}]^f\}^0 \ . \tag{B3}$$

We next use Eq. (B3) in Eq. (3.2). If we expand the delta function in Eq. (3.2) and recouple we obtain

$$\mathcal{F}^i_{\Lambda M_\Lambda}(R)\equiv\int Y_{\Lambda M_\Lambda}(\hat{\mathbf{R}}')\langle f|D_i(\mathbf{k}',\mathbf{k};\mathbf{r}')|i\rangle d\hat{\mathbf{R}}'\delta(\mathbf{R}'-\mathbf{R})$$
$$=\sum_{\lambda\alpha\lambda'\beta}A_i(\lambda\alpha\lambda'\beta)\sum_{\nu Kf}\left[\frac{2K+1}{(2f+1)(2\Lambda+1)}\right]^{1/2}\{[[\mathbf{k}\otimes\mathbf{k}']^\lambda\otimes Y_\nu(\hat{\mathbf{Q}})]^f\otimes\tilde{f}_K(\lambda\alpha\lambda'\beta;\Lambda,f,\nu,R)\}^{\Lambda M_\Lambda}, \tag{B4}$$

where

$$\tilde{f}_{KM_K}(\lambda\alpha\lambda'\beta;\Lambda,f,\nu,R)=\left\langle f|\bar{d}_i(\alpha,\mathbf{r}')i^\nu j_\nu(Qr')\frac{\delta(R-R')}{R^2}\right.$$
$$\times\sum_{\mathcal{K}}(-)^{\alpha+\lambda+\lambda'+\mathcal{K}}\sqrt{(2\nu+1)(2f+1)(2\mathcal{K}+1)(2\alpha+1)}$$
$$\left.\times\begin{bmatrix}\nu&\alpha&\mathcal{K}\\0&0&0\end{bmatrix}\begin{Bmatrix}\nu&\mathcal{K}&\alpha\\\lambda'&\lambda&f\end{Bmatrix}\{Y_\Lambda(\hat{\mathbf{R}})\otimes[Y_{\mathcal{K}}(\hat{\mathbf{r}}')\otimes S^{\lambda'}_\beta]^f\}^{KM_K}|i\right\rangle. \tag{B5}$$

Again we recognize that for transitions between states having total angular momentum $I=0$, the only allowed value of K is $K=0$, implying $\Lambda=f$. For the calculations in this paper we have retained only the monopole density corresponding to $\Lambda=0$. We therefore also have $f=0$ and $\nu=\lambda$, $\mathcal{K}=\lambda'$. Thus, Eq. (B4) becomes

$$\mathcal{F}^i_{00}=\sum_{\substack{\lambda\alpha\lambda'\beta\\\Lambda}}A_i(\lambda\alpha\lambda'\beta)[[\mathbf{k}\otimes\mathbf{k}']^\lambda\otimes Y_\lambda(\hat{\mathbf{Q}})]^{00}\tilde{f}_0(\lambda\alpha\lambda'\beta;\Lambda0\lambda;R), \tag{B6}$$

where

$$\tilde{f}_0(\lambda\alpha\lambda'\beta;00,\nu;R)=\delta(\lambda,\nu)\langle f|i^\nu j_\nu(Qr')\bar{d}_i(\alpha,\mathbf{r}')\frac{\delta(R-R')}{R^2}\frac{(-)^{\lambda'}}{\sqrt{4\pi}}\sqrt{2\alpha+1}\begin{bmatrix}\nu&\alpha&\lambda'\\0&0&0\end{bmatrix}[Y_{\lambda'}(\hat{\mathbf{r}}')\otimes S^{\lambda'}_\beta]^{00}|i\rangle. \tag{B7}$$

As long as we consider only forward scattering, $\lambda=\lambda'=1$ cannot contribute and we therefore drop these terms.

To calculate the amplitude $\mathcal{F}^i_{00}$ in Eq. (B6) we note that there are terms with $\lambda=0$ and $\lambda=2$. The term $\lambda=0$ is the same as that worked out in Sec. III. The one with $\lambda=2$ is a new term. So, we have

$$\mathcal{F}^i_{00}=\left\{\sum_{\alpha\beta}A_i(0\alpha\alpha\beta)\left(-\frac{1}{\sqrt{3}}\right)\mathbf{k}'\cdot\mathbf{k}\tilde{f}_0(0\alpha\lambda'\alpha;000;R)+\sum_{\alpha\lambda'\beta}A_i(2\alpha\lambda'\beta)\sqrt{3/2}(\mathbf{k}\cdot\hat{\mathbf{Q}}\cdot\mathbf{k}'\cdot\hat{\mathbf{Q}}-\tfrac{1}{3}\mathbf{k}'\cdot\mathbf{k})\tilde{f}_0(2\alpha\lambda'\beta;002;R)\right\}\frac{1}{\sqrt{4\pi}}. \tag{B8}$$

To include the second term of Eq. (B8) in the calculation, we assume that the scattering occurs in the forward direction. This term is very large for SEQ.

APPENDIX C: OPERATOR DISTORTIONS

In the body of the paper we have assumed that the initial and final pions are in plane-wave states. The physical states are, of course, not plane waves and, in fact, are strongly attenuated as the pion penetrates into the nucleus. This means that in practice the momenta $\mathbf{k}$ and $\mathbf{k}'$ to be used in the amplitude of Eq. (3.3) are not the asymptotic momenta but rather the pion momenta inside the medium. In this appendix we want to estimate the effect of evaluating $\mathbf{k}$ and $\mathbf{k}'$ as local momenta. This correction will affect our evaluation of both DINT and SEQ.

Consider first the correction for DINT, Fig. 1(a). In this case the second term in Eq. (B8) vanishes in the plane wave limit, since $j_2(qr)=0$ when $q=0$. However, when we include distorted waves q may no longer be taken to vanish. We will next estimate $\mathbf{q}$ and q^2 in the Eikonal approximation. For this we take the distorted waves to be

$$\psi^{(+)}=e^{i\mathbf{k}\cdot\mathbf{r}}e^{-i/2k\int_{-\infty}^{z}U(b,z')dz'},$$
$$\psi^{(-)*}=e^{-i\mathbf{k}'\cdot\mathbf{r}}e^{-i/2k\int_{z}^{\infty}U(b,z')dz'}, \tag{C1}$$

where U is the equivalent local potential. We next make use of the fact that k^n acting on $\psi(k)$ becomes, in coordinate space, $(-i)^n\nabla^n\psi(r)$. We find

$$\nabla\psi^{(+)}=i(\mathbf{k}-\delta\mathbf{k})\psi^{(+)},$$
$$\nabla\psi^{(-)*}=-i(\mathbf{k}'+i\delta\mathbf{k}')\psi^{(-)*}, \tag{C2}$$

where in Eqs. (C1) and (C2) the momentum $\mathbf{k}$ and $\mathbf{k}'$ are now those in free space

$$\delta\mathbf{k}=-\frac{i}{2k}\left[\hat{\mathbf{z}}U(b,z)+\hat{\mathbf{e}}_b\int_{-\infty}^{z}dz'\frac{\partial}{\partial b}U(b,z')dz'\right], \tag{C3}$$

$$\delta\mathbf{k}'=-\frac{i}{2k}\left[-\hat{\mathbf{z}}U(b,z)+\hat{\mathbf{e}}_b\int_{z}^{\infty}dz'\frac{\partial}{\partial b}U(b,z')dz'\right].$$

Here $\hat{\mathbf{z}}$ is a unit vector in the $\hat{\mathbf{z}}$ direction and $\hat{\mathbf{e}}_b$ a unit vector in the direction of the impact parameter. From this we find

$$q=\mathbf{k}'-\mathbf{k}\rightarrow\mathbf{q}+i(\delta\mathbf{k}'+\delta\mathbf{k})$$
$$=\mathbf{q}+\frac{1}{2k}\hat{\mathbf{e}}_b\int_{-\infty}^{\infty}dz'\frac{\partial}{\partial b}U(b,z')\ . \tag{C4}$$

Note that in the forward direction q is perpendicular to $\mathbf{k}$ and $\mathbf{k}'$, even with the medium modifications, so that the correction term in Eq. (B8) becomes to leading order in U

$$\mathbf{k}\cdot\mathbf{Q}\mathbf{k}'\cdot\mathbf{Q}-\tfrac{1}{3}\mathbf{k}'\cdot\mathbf{k}\rightarrow-\tfrac{1}{3}\mathbf{k}'\cdot\mathbf{k}\ . \tag{C5}$$

We have taken $\mathbf{Q}=\mathbf{q}/2$ for DINT according to Table II. Now we want to estimate q^2 for forward scattering. We find

$$\psi^{(-)*}q^2\psi^{(+)}\rightarrow-\frac{1}{2k^2}\psi^{(-)*}\psi^{(+)}\left\{U^2(b,z)+\left[\int_{-\infty}^{z}\frac{\partial}{\partial b}U(b,z')dz'\right]\left[\int_{z}^{\infty}\frac{\partial}{\partial b}U(b,z')dz'\right]\right\}\ . \tag{C6}$$

We estimate this by observing that the largest contribution to the DWIA integrals occurs in the surface near $b\simeq\bar{b}$, and there we may take[32]

$$U(b,z)\simeq U(b)e^{-(r-b)/a}\simeq U(b)e^{-z^2/2ab}\ ,$$
$$U(b)\simeq U(\bar{b})e^{-(b-\bar{b})/a}\ , \tag{C7}$$
$$\sqrt{2\pi a\bar{b}}\,\frac{\mathrm{Im}U(\bar{b})}{2k}=-1\ .$$

Using these approximations, we find

$$\langle q^2\rangle\rightarrow\frac{1}{2k^2}\left\{-U^2(\bar{b})+\left[\frac{\pi a\bar{b}}{2}\right]\left[\frac{1}{\bar{b}}-\frac{1}{a}\right]^2U^2(\bar{b})\right\}$$
$$\simeq-0.63\ \mathrm{fm}^{-2}\ . \tag{C8}$$

To estimate the size of the corrections for DINT we have replaced

$$j_0(qr/2)\rightarrow1-\tfrac{1}{24}q^2r^2=1+0.01k^2r^2\ , \tag{C9}$$
$$j_2(qr/2)\rightarrow-0.08j_2(kr)\ , \tag{C10}$$

which gives the correct expressions near resonance ($k^2=2\ \mathrm{fm}^{-2}$) to order q^2. The correction to the Bessel function $j_0(qr)$ has been estimated by evaluating the average value of $r^2\rho^2(r)$ along an Eikonal trajectory at impact parameter $\bar{b}$. Since the dominant r dependence comes from the factors of density in the transition amplitude, we average this quantity over the square of the density, using Eq. (C7) for the dependence of $\rho(z)$. We then find that the correction in Eq. (C9) is on the order of 1% in the amplitude. To estimate the correction in $j_2(qr)$ we have used Eq. (C10), and find a modification of a few percent. We conclude that the uncertainties arising from the operator distortions for DINT are well within those arising from other sources.

To estimate the corrections for SEQ we take $\mathbf{k}$, $\mathbf{k}'$, and $\hat{\mathbf{Q}}$ colinear and then the tensor

$$\mathbf{k}\cdot\hat{\mathbf{Q}}\mathbf{k}'\cdot\hat{\mathbf{Q}}-\tfrac{1}{3}\mathbf{k}\cdot\mathbf{k}'\cong\tfrac{2}{3}\mathbf{k}\cdot\mathbf{k}'\ .$$

Now, the leading correction to K^2 is linear in U and we find

$$\langle K^2\rangle\simeq k^2-U=k^2+0.74\ \mathrm{fm}^{-2} \tag{C11}$$

for $b\cong\bar{b}$. This amounts to about a 20% increase in the effective k at resonance. Because the strongest energy dependence occurs through the distorted waves and the Δ_{33} propagator, which are unaffected by this correction in Eq. (C11), we do not believe that this shift is a very significant correction. In any case, we have not included this effect in the calculation, and it is therefore an additional source of uncertainty in our estimate of SEQ.

*Present address: Argonne National Laboratory, Argonne, IL 60439.

[1]M. Hirata, J.-H. Koch, F. Lenz, and E. J. Moniz, Phys. Lett. **70B**, 281 (1977); E. Oset and W. Weise, Phys. Lett. **27B**, 159 (1978).
[2]D. J. Ernst and M. B. Johnson, Phys. Rev. C **32**, 940 (1985).
[3]R. Dymarz and F. C. Khanna, Phys. Rev. Lett. **56**, 1448 (1986).
[4]M. B. Johnson, E. R. Siciliano, H. Toki, and A. Wirzba, Phys. Rev. Lett. **52**, 593 (1984).
[5]R. Gilman, H. T. Fortune, M. B. Johnson, E. R. Siciliano, H. Toki, and A. Wirzba, Phys. Rev. C **32**, 349 (1985).
[6]R. Gilman, H. T. Fortune, M. B. Johnson, E. R. Siciliano, H. Toki, A. Wirzba, and B. A. Brown, Phys. Rev. C **34**, 1895 (1986).
[7]T. Karapiperis and M. Kobayashi, Ann. Phys. (N.Y.) **177**, 1 (1987).
[8]E. Oset, M. J. Vicente-Vacas, M. B. Johnson, D.Strottman, H. T. Fortune, and R. Gilman, Nucl. Phys. **A483**, 514 (1988).
[9]S. J. Greene, *et al.*, Phys. Rev. C **25**, 927 (1982).
[10]L. C. Bland, R. Gilman, M. Carchidi, K. Dhuga, C. L. Morris, H. T. Fortune, S. J. Greene, P. A. Seidl, and C. F. Moore, Phys. Lett. **128B**, 157 (1983); C. L. Morris, H. T. Fortune, L. C. Bland, R. Gilman, S. J. Greene, W. B. Cottingame, D. B. Holtkamp, G. R. Burleson, and C. F. Moore, Phys. Rev. C **25**, 3218 (1982).
[11]R. Gilman, Los Alamos National Laboratory Report No. LA-10524-T, 1985.
[12]D. Koltun and M. K. Singham, Phys. Rev. C **39**, 704 (1989).
[13]G. A. Miller, Phys. Rev. Lett. **53**, 2008 (1984).
[14]M. B. Johnson and L. S. Kisslinger, Phys. Lett. **168B**, 26 (1986).
[15]G. E. Brown and W. Weise, Phys. Rep. **22**, 279 (1975).
[16]T. Hippchen, J. Speth, and M. B. Johnson, Phys. Rev. C **40**, 1316 (1989).
[17]D. Brink and G. R. Satchler, *Angular Momentum* (Oxford University Press, London, 1968).

[18]E. R. Siciliano, M. B. Johnson, and H. Sarafian, submitted to Ann. Phys. (N.Y.).
[19]M. B. Johnson and H. A. Bethe, Nucl. Phys. **A305**, 418 (1977).
[20]G. E. Brown, S. O. Bäckman, E. Oset, and W. Weise, Nucl. Phys. **A286**, 191 (1977).
[21]R. A. Eisenstein and G. A. Miller, Comput. Phys. Commun. **11**, 95 (1976).
[22]M. B. Johnson and E. R. Siciliano, Phys. Rev. C **27**, 1647 (1983).
[23]W. B. Cottingame and D. B. Holtkamp, Phys. Rev. Lett. **45**, 1828 (1980).
[24]T. A. Brody and M. Moskinsky, *Tables of Transformation Brackets for Shell Model Calculations* (Gordon and Breach, New York, 1960).
[25]A. P. Zuker, B. Buck, and J. B. McGrory, Phys. Rev. Lett. **21**, 31 (1968).
[26]J. B. McGrory and B. H. Wildenthal, Phys. Rev. C **7**, 974 (1973).
[27]The TBTD matrix elements are defined in B. A. Brown, W. A. Richter, and N. S. Godwin, Phys. Rev. Lett. **45**, 1681 (1980). Note that the TBTD are doubly reduced and specified in the Edmonds convention. We need matrix elements reduced in spin only in the convention of Ref. 17. This accounts for the factors on the left-hand side of Eqs. (5.2) and (5.3).
[28]A. Etchegoyen, W. D. M. Rae, N. S. Godwin, and B. A. Brown, Michigan State Cyclotron Laboratory Report No. 524, 1985.
[29]T.-S. H. Lee, D. Kurath, and B. Zeidman, Phys. Rev. Lett. **39**, 1307 (1977).
[30]S. J. Greene, C. J. Harvey, P. A. Seidl, R. Gilman, E. R. Siciliano, and M. B. Johnson, Phys. Rev. C **30**, 2003 (1984).
[31]M. Gmitro, J. Kvasil, and R. Mach, Phys. Rev. C **31**, 1349 (1985).
[32]M. B. Johnson and H. A. Bethe, Comments Nucl. Part. Phys. **8**, 75 (1978).